plant biology

Plant Biology ISSN 1435-8603

RESEARCH ARTICLE

Time-series multi-omics analysis of micronutrient stress in *Sorghum bicolor* reveals iron and zinc crosstalk and regulatory network conservation

A. Mishra[1], A. Bhat[2], S. Kumari[3], R. Sharma[2], J. Braynen[3], D. Tadesse[2], S. El Alaoui[4], S. Seaver[4], N. Grosjean[5], D. Ware[3,6], M. Xie[2] & T. Paape[7,8]

1 Institute for Advancing Health Through Agriculture, Texas A&M, College Station, Texas, USA
2 Brookhaven National Laboratory, Upton, New York, USA
3 Cold Spring Harbor Laboratory, Cold Spring Harbor, New York, USA
4 Argonne National Laboratory, Lemont, Illinois, USA
5 Lawrence Berkeley National Laboratory, Berkeley, California, USA
6 USDA-ARS-NAA, Ithaca, New York, USA
7 Department of Soil and Crop Sciences, Texas A&M, College Station, Texas, USA
8 USDA-ARS Responsive Agriculture Food Systems Research Unit, College Station, Texas, USA

Keywords
Differential expression; gene regulatory network; iron; sorghum; zinc.

Correspondence
T. Paape, USDA-ARS Responsive Agriculture Food Systems Research Unit, College Station, Texas, USA.
E-mail: timothy.paape@usda.gov, tim.paape@ag.tamu.edu
M. Xie, Brookhaven National Laboratory, Upton, NY, USA.
E-mail: mxie@bnl.gov

Editor
R. Giehl

Received: 28 February 2025;
Accepted: 29 March 2025

doi:10.1111/plb.70038

ABSTRACT

- Micronutrient stress impacts growth, biomass production, and grain yield in crops. Multi-omics studies are valuable resources in identifying genes for functional studies and trait improvement, such as accumulation of Fe or Zn under deficient or excess conditions for bioenergy or grain agriculture.
- We conducted transcriptomics and ionomics analyses on *Sorghum bicolor* BTx623, grown under Fe and Zn limited and excess conditions over a 21-day period. To identify early and late transcriptional response in roots and leaves, 180 RNAseq libraries were sequenced for differential expression and co-expression network analyses. Fe and Zn accumulation was measured using ICP-MS at each time point, and a fluorometer was used to estimate chlorophyll content in leaves.
- Among the four treatments, Fe limitation and Zn excess resulted in the largest phenotypic effects and transcriptional response in roots and leaves. Several of the reduction (Strategy I) and chelation (Strategy II) strategy genes that improve bioavailability of Fe and Zn in plant roots often used by non-grass and grass species, respectively, were differentially expressed. Gene regulatory network (GRN) analysis of roots revealed enrichment of genes from Fe limiting and Zn excess which strongly connect to homologues of *SbFIT*, *SbPYE*, and *SbBTS* as hub genes. The GRN for leaf responses showed homologues of *SbPYE* and *SbBTS* as hubs connecting genes for chloroplast biosynthesis, Fe-S cluster assembly, photosynthesis, and ROS scavenging.
- Expression analyses suggest sorghum uses Strategy II genes for Fe and Zn uptake, as expected, but can also utilize Strategy I genes, which may be advantageous in variable moisture environments. We found strong overlap between Fe and Zn responsive GRNs, indicative of micronutrient crosstalk. We also found conservation of root and leaf GRNs, and known homologous genes suggest strong constraints on homeostasis networks in plants. These data will provide a resource for functional genetics to enhance micronutrient transport in sorghum, and opportunities to conduct further comparative GRN analysis across diverse crops species.

INTRODUCTION

The micronutrients iron (Fe) and zinc (Zn) are essential for plant growth and development, and their uptake and transport involve polygenic gene networks that function to maintain nutrient homeostasis. Essential micronutrients, such as Fe and Zn, are needed in relatively small amounts compared to macronutrients, such as nitrogen (N) and phosphorus (P), but their limited bioavailability in soil is nevertheless a challenge for maximizing production. Important plant processes, including photosynthesis and water-use efficiency, depend on the availability of these metal ions. Both Fe and Zn are indispensable cofactors for critical aspects of plant growth, including numerous metabolic pathways, post-translational modifications, cell wall biosynthesis, and macronutrient (e.g., C and N) assimilation (Marschner & Marschner 2012). Moreover, biofortification of Fe and Zn to improve nutritional qualities of grains is a focus of breeding efforts in all major crops (Stangoulis & Knez 2022). To address deficiencies in essential nutrients in crops, application of fertilizers and soil amendments are often

necessary, but can be harmful to the environment and increase production costs.

Plants overcome the limited bioavailability of Fe chelates beginning in the roots. Land plants have evolved two main strategies to cope with Fe deficiency and to optimize Fe uptake, known as Strategy I and Strategy II, utilized by different species of non-grasses and grasses, respectively (Marschner & Römheld 1994). Non-grass species, such as *Arabidopsis thaliana*, use Strategy I (acidification–reduction strategy) where increased proton extrusion into the rhizosphere lowers soil pH to solubilize Fe^{3+} through P-type ATPases (*AHA*, *HMAs*). The bioavailability of iron to the plant is further facilitated by converting Fe^{3+} to Fe^{2+} at the root surface where Ferric Reductase Oxidase 2 (*FRO2*) protein acts as a Fe-chelate reductase on the plasma membrane (Robinson *et al.* 1999). Following reduction, Iron Regulated Transporter 1 (*IRT1*) transports Fe^{2+} ions into root cells (Eide *et al.* 1996; Vert *et al.* 2002). Grass species, such as barley, maize, rice, sorghum, and wheat, are all presumed to use Strategy II (chelation strategy), which involves the secretion of phytosiderophores (PSs) from roots into the rhizosphere (Negishi *et al.* 2002). PSs are mugineic acid (MAs) derivatives synthesized from S-adenosyl methionine (*SAM*). Strategy II transport mechanisms have been well studied in *Oryza sativa* (rice) where transporter of mugineic acids (*TOM*) secretes PSs (Nozoye *et al.* 2011) into the rhizosphere where they chelate Fe^{3+}. Intact Fe(III)-PS complexes can then be transported into root cells through yellow stripe-like (*YSL*) transmembrane proteins (Von Wiren *et al.* 1996; Curie *et al.* 2001).

In rice and barley, ionomics and transcriptomics analyses suggest that they use a combination of Strategies I and II, but can employ either strategy, depending on their local environments, which vary seasonally and globally from very wet to very dry soils (Wairich *et al.* 2019; Zhong *et al.* 2022; Aksoy 2024). However, it is not yet known whether other grass crop species, such as sorghum or maize, use a similar combined strategy for Fe uptake. A comparative co-expression network analysis between *A. thaliana* and *O. sativa* showed that the Fe-responsive transcriptional networks were largely conserved between these two plant species, despite the different Fe uptake strategies adopted by these species (Grillet & Schmidt 2019). Together these studies suggest plasticity in Fe uptake strategies, and functionally homologous genes from both strategies must be present across widely diverged plant species if combined strategies are environmentally dependent. Moreover, it suggests that Fe uptake and homeostasis pathways are likely to be conserved among grasses and non-grasses.

In vascular plants, our knowledge of Fe and Zn transport and homeostasis as polygenic gene regulatory networks (GRN) has come primarily from studies in *A. thaliana* (Kim *et al.* 2019; Spielmann *et al.* 2023). Metal ion uptake and transport systems in plants include a series of complex regulatory networks that involve a group of transcription factors (TFs) from the basic helix loop helix (bHLH) family (Hao *et al.* 2021; Gao & Dubos 2024). Over the past decade, several studies have reported the direct or indirect involvement and interdependency of at least one bHLH on other members of the group for active involvement in metal ion uptake and homeostasis (Zhang *et al.* 2015, Li *et al.*, 2016; Liang *et al.*, 2017). A thorough characterization of the bHLH TF family in *A. thaliana* identified 16 bHLH family members for their active involvement in the regulatory cascade of Fe transport and homeostasis (Colangelo and Guerinot, 2004; Wang *et al.*, 2007; Yuan *et al.*, 2008; Wang *et al.*, 2013; Zhang *et al.* 2015; Maurer *et al.*, 2014; Cui *et al.*, 2018). Upstream of the structural genes involved in metal ion uptake and homeostasis are four bHLH TFs belonging to clade Ib: *ORG2* (bHLH39), *ORG3* (bHLH38), bHLH100, and bHLH101 (Gao & Dubos 2024). These TFs are known to form heterodimers with *FIT* (Fe-deficiency Induced Transcription Factor) from clade IIIa, which transcriptionally activate downstream genes in response to Fe deficiency. However, members of clade IVc and clade IVb, which includes *POPEYE* (*PYE*, bHLH47), are known to heterodimerize to repress the transcription of downstream genes (Colangelo and Guerinot, 2004; Yuan *et al.*, 2008; Wang *et al.*, 2013; Maurer *et al.*, 2014). Another key regulator of Fe and Zn binding is *BRUTUS* (*BTS*). This was first characterized in *A. thaliana* for its role in ubiquitination of bHLH proteins under Fe sufficiency conditions (Long *et al.* 2010; Connorton *et al.* 2017; Hindt *et al.* 2017). Moreover, Kobayashi *et al.* (2013) found that *BTS* orthologs in rice (*HRZ1* and *HRZ2*) function similarly to *AtBTS*, and other orthologs of the *A. thaliana* bHLH family of TFs play a large role in metal ion homeostasis (Liang 2022; Li *et al.* 2019).

Approximately 80% of cellular Fe found in green leaves is located in the chloroplasts (Jacobson, 1945), where membrane-bound complexes require Fe to function (López-Millán *et al.*, 2016). The typical result of Fe deficiency is chlorosis, caused by a lack of chlorophyll, which has negative impacts on photosynthesis (Vert *et al.* 2002; Tabata *et al.* 2022). The same chemical properties that make Fe essential for metabolism, such as redox properties and serving as cofactors for various enzymes, can also make Fe highly toxic. In excess, unchelated Fe species can be cytotoxic by reacting with hydrogen peroxide and generating reactive oxygen species (ROS), leading to oxidative stress. Deficiency and toxicity symptoms can arise when the transport of metal ions exceeds the ability to maintain homeostasis. Understanding how nutrient stress affects chloroplast-related processes is important for bioenergy sorghum, where plant biomass requires efficient photosynthesis, as well as grain sorghum, which requires sufficient resource allocation to panicles for high yields.

Like Fe, Zn is involved in fundamental biological processes, including transcription, translation, gene regulation, carbon concentrating mechanisms, and CO_2 fixation, and is a crucial cofactor of enzymes (Suganya *et al.* 2020). For example, Zn is an essential cofactor for most classes of carbonic anhydrase (Sasaki *et al.* 1998) and for correct RuBisCO folding. As a result, symptoms of Zn deficiency in plants include reduced photosynthetic activity, discoloration of leaves, and reduced biomass and yield, as shown in *S. bicolor* (Li *et al.* 2013). As a protein cofactor, Zn is prevalent in hydrolytic enzymes, where it provides a chemical functionality that is not easily provided with amino acid side chains, and it is commonly used to stabilize protein structures. Zn and Fe often compete for uptake by plant roots. Both elements are taken up by similar transporters in the root system, which can lead to competitive inhibition. Moreover if one of the metals is in excess, it can affect the availability and uptake of the other (Hanikenne & Bouché 2023). Furthermore, Fe and Zn deficiencies can alter the expression of genes and TFs involved in metal homeostasis. For example, Fe deficiency often induces the expression of genes that increase both Fe and Zn uptake and

transport, using the regulatory mechanisms described above (e.g., *BTS*, *PYE*, *FIT*) (Stanton *et al.* 2023).

Sorghum (*S. bicolor*) is grown as both grain and bioenergy crops and is an annual C_4 grass that is tolerant to drought and variable edaphic conditions (Mullet *et al.* 2014; Khalifa & Eltahir 2023). Grain sorghum has been the focus of ongoing biofortification efforts of micronutrients, including Fe and Zn (Kumar *et al.* 2015; Gaddameedi *et al.* 2022). For both grain and bioenergy sorghum, transition metals such as Fe and Zn are essential nutrients for plant growth and productivity, but excess can lead to toxicity and deficiencies lead to chlorotic disease and loss of photosynthesis. Responses to environmental stresses, such as climate and salinity, are tractable using multi-omics approaches in sorghum (Ren *et al.* 2022; Mukherjee *et al.* 2024). Micronutrient stress can be measured over time using ionomics, transcriptomics, and phenomics, which is a first step toward understanding gene function and systems-level processes involving multiple interacting proteins. While sorghum is commonly considered a highly drought tolerant crop species, it has a global distribution that spans the arid, tropical to subtropical environments which vary widely in rainfall (Hodnett *et al.* 2020), and is also known to experience waterlogging (Khalifa & Eltahir 2023). Heavy periods of rain and flooding can result in submergence, soil saturation, anoxia, and hypoxia, much like rice paddy fields (Wairich *et al.* 2019). This environmental variability suggests the possibility of gene expression responses from both strategies of micronutrient uptake.

To address Fe and Zn nutrient transport into roots and from roots to shoots, we conducted a time-series investigation of *S. bicolor* Btx623 grown under conditions of Fe or Zn limitation or excess to identify patterns of ion accumulation or deficiencies, and corresponding transcriptomic responses in leaves and roots over a 3-week period. We used the root transcriptomics data to explore the homologous genes commonly involved in Fe and Zn transport to study whether conservation of genes from grasses and non-grasses may be involved in micronutrient uptake. We also examined the transcriptomic responses of Fe and Zn stress on chloroplast function, based on transcriptomic and fluorometer data. Recent progress on Fe-related gene annotations and gene ontologies has provided lists of genes that have been implicated in Fe and Zn transport in *A. thaliana* that can be used to search for homologues in crop species (Mai *et al.* 2023). In rice, the search for Fe related homologous genes known in *A. thaliana* has been useful to identify differentially expressed genes (DEGs), and comparison of conserved co-expression networks across species (Grillet & Schmidt 2019; Wairich *et al.* 2019). We therefore used homology of *A. thaliana* orthologs as a starting point to identify genes of interest, under the assumption that Fe and Zn homeostasis may be largely conserved networks in land plants. Using these data, we conducted co-expression analyses to construct GRNs to (i) characterize Fe and Zn regulatory networks in sorghum, (ii) identify possible signals of conservation among the Fe and Zn networks, and (iii) describe their similarity to other grass and non-grass species. This study will provide valuable information on the regulatory mechanisms of Fe and Zn uptake and transport to further formulate hypotheses for functional genomics studies and to improve nutritional qualities and increased resilience in both grain and bioenergy sorghum.

MATERIAL AND METHODS

Plant growth and sample collection

Seeds of *Sorghum bicolor* cv. BTx623 were germinated on filter paper in 6-cm Petri dishes, then transplanted to a hydroponic growth system with temperature settings of 21–27°C in a greenhouse. *S. bicolor* cv. BTx623 seedlings were transplanted into modified Hoagland's solution (1.25 mM KNO_3, 1.25 mM $Ca(NO_3)_2$, 250 μM NH_4NO_3, 500 μM $MgSO_4$, 250 μM KH_2PO_4, 50 μM H_3BO_3, 10 μM $MnSO_4$, 0.2 μM $CuSO_4$, 0.5 μM Na_2MoO_4, 1 μM $ZnSO_4$, 50 μM NaFe(III)EDTA, pH 5.6) 7 days after germination. After a 3-week acclimation in the hydroponic system, seedlings were randomized and transplanted into modified Hoagland's solutions with different $ZnSO_4$ and NaFe(III) EDTA concentrations: control solution (1 μM $ZnSO_4$, 50 μM NaFe(III)EDTA), Zn deficiency (ZnLim) solution (0 μM $ZnSO_4$, 50 μM NaFe(III)EDTA), excess Zn (ZnEx) solution (100 μM $ZnSO_4$, 50 μM NaFe(III)EDTA), Fe deficiency (FeLim) solution (1 μM $ZnSO_4$, 0 μM NaFe(III)EDTA), and excess Fe (FeEx) solution (1 μM $ZnSO_4$, 1 mM NaFe(III)EDTA). Samples for RNA extraction were collected between 10:00 h and 12:00 h from three individual plants to represent three biological replicates. Leaf and root samples were collected at the same time points in parallel for RNA extraction and ICP-MS measurements. In total, 181 samples of sorghum were collected for phenotypic measurements and RNAseq.

Phenotype measurements using ICP-MS and leaf measurements of chlorosis

The leaf and root tissues were collected at time points 0 h, 1 h, 2 days, 4 days, 7 days, 14 days, and 21 days after the start of the treatments. To wash off the excess metals from root samples, they were sequentially immersed in 5 mM $CaCl_2$, 1 mM MES-KOH, and ultra-pure H_2O (UPW) for 30 min each. Subsequently, the samples were dried by placing them in a 50°C oven for a minimum of 48 h. Once the samples were dried and homogenized via crushing, approximately 75 mg was weighed and transferred into tubes for digestion by adding ICP-MS grade 69% HNO_3 (1017992500, Sigma-Aldrich, St. Louis, MO, USA). They were allowed to stand overnight (to avoid boiling over) and then transferred on a Digiprep heat-block set at 95°C for 4–5 h. Finally, the samples were diluted four-fold with UPW and were ready for analysis. We used ICP-MS (NexION 350D Model; Perkin Elmer, Waltham, MA, USA) to determine the concentrations of several elements including Boron (B), Sodium (Na), Magnesium (Mg), Aluminium (Al), Phosphorus (P), Sulfur (S), Potassium (K), Calcium (Ca), Iron (Fe), Manganese (Mn), Cobalt (Co), Nickel (Ni), Copper (Cu), Zinc (Zn), Arsenic (As), Selenium (Se), Rubidium (Rb), Strontium (Sr), Molybdenum (Mo), and Cadmium (Cd) in the samples. The instrument was calibrated using an environmental standard mix (N9307805, Perkin Elmer), and ^{89}Y and ^{115}In were used as internal standards (M1-ISMS-25, Elemental Scientific) in the process. Eventually, the concentrations were converted from μL g^{-1} to μg g^{-1} by normalizing to dry weights of the samples, respectively. We analysed the phenotype data using ANOVA and linear models in R to identify significant changes between control and treatments, and to identify the time points with the largest changes in ion accumulation and other stress related phenotypes.

RNA isolation, RNA-seq and RT-qPCR

Total RNA was extracted from root and leaf samples using the Spectrum Plant Total RNA kit (Sigma-Aldrich). Approximately 100 mg ground tissues were lysed in 850 µL preheated CTAB buffer. Proteins were removed by mixing with 600 µL chloroform-isoamyl alcohol (24:1 v:v). After centrifugation, the supernatant was passed through the filter column provided in the Spectrum Plant Total RNA kit (Sigma-Aldrich) and total RNAs were extracted following the manufacturer's manual. A total of 181 RNAseq libraries from sorghum samples were generated and sequenced by Texas A&M University Genomics and Bioinformatics Service (https://www.txgen.tamu.edu) using Perkin Elmer Nextflex Rapid Directional RNA-seq kit 2.0, including Nextflex Poly-A-Selection 2.0 beads for polyA enrichment. All 181 samples were sequenced using a 2X150 v.1.5 bp paired end (PE) approach and four lanes on an Illumina Novaseq 6000 S4 instrument targeting 20–30 million reads per sample. For mapping reads we used *S. bicolor* v. 3.1BTx623 (Cooper *et al.*, 2019). reference genome (https://phytozome-next.jgi.doe.gov/info/Sbicolor_v3_1_1). RNAseq data were analysed with the DRAGEN Bio-IT Platform (v. 3.8) using default parameters.

We used RT-qPCR to validate the expression of two genes: Sobic.009G222200 (*SbOPT3*) and Sobic.001G087700 (*SbBTS*). We used 500 ng total RNA to synthesize cDNA with RevertAid Reverse Transcriptase (ThermoFisher Scientific, Hillsboro, OR, USA) using an oligo-dT primer. An aliquot of 2 µl five-fold diluted cDNA was used for qPCR. The constitutively expressed Sb*ELF6* (Sobic.001G048200) gene was used as an endogenous control. The gene expressions before any treatments (0 h) were set as 1. Values in the figures (Fig. S4) represent mean ± SD, $n = 3$. We determined *P*-values by comparing with Fe- or Zn-treated samples at each time point using a two-tail Student *t*-test. The used primers are: *SbOPT3* (5′-CCAACATCGCCACATGGCTGG-3′ and 5′-CATGAA GGCGGTGCCGGCGTC-3′), *SbBTS* (5′-GTCGGTCCAAAT TGCCAATCC-3′ and 5′-ATCAGTGCCCAATCCACTCC-3′) and *SbELF6* (5′-TGAAGCGGGTGAGAAGATTGT-3′ and 5′-AGCCAAATCATACTCGCCCA-3′).

Differential expression and homologous gene analysis

We used principal components analysis (PCA) to identify outliers in our replicates and assess sample quality prior to running differential expression analysis. We removed one FeEx 7-day root sample and one FeEx 14-day leaf sample from the *S. bicolor* dataset because these libraries had $<10^6$ total raw read counts. All remaining samples were included in subsequent analyses. Throughout the time-series experiment, plants were sampled that were growing in a control hydroponic chamber (see previous section; Methods describing treatment concentrations) that was used for differential expression analysis of the excess or limiting treatments at any of the time points, so that temporal variation in the controls had similar-aged plants for statistical comparisons. The identification of DEGs between control and treatment samples was performed with the DESeq R package (v. 1.40.2) using the recommended, default settings where genes with a |log2 fold-change| ≥ 1 and an adjusted *P*-value <0.05 were considered differentially expressed.

We used Phytozome (Goodstein *et al.* 2012) gene annotations for the *S. bicolor* v. 3.1.1 genome (https://phytozome-next.jgi.doe.gov). In Phytozome, the between species annotations were created using Inparanoid pairwise orthology, and paralogy groups have been calculated across all proteomes in their database, and best BLAST hit to *A. thaliana*. The short names from *A. thaliana* TAIR genes come from the Phytozome annotation file. We also conducted a gene tree analysis using homologues generated by the Ensembl Compara pipeline. This pipeline uses maximum likelihood, generated by TreeBeST (Tree Building guided by Species Tree) method (Vilella *et al.* 2009). Using the gene trees, we generated homologue pairs of Poplar–Sorghum; Poplar–Arabidopsis, Sorghum–Arabidopsis, which were further differentiated among 1-to-1 homologues; 1-to-many homologues; many-to-many homologues. Only the homologue pairs that had minimum 20% identity were selected as homologous pairs for the downstream analysis. Finally, we used BLAST of our focal candidate genes in *S. bicolor* using TAIR (https://www.arabidopsis.org/tools/blast/), JGI/Phytozome (https://phytozome-next.jgi.doe.gov/blast-search), and Ensembl (www.ensembl.org). When reporting homology using *A. thaliana* gene nomenclature, we realize that future functional analyses may provide more accurate gene IDs for *S. bicolor*.

Gene regulatory network and co-expression analysis

The SimpleTidy GeneCoEx package in R was used to construct the GRN and co-expression analysis (Li *et al.* 2023) for FeLim and ZnEx stress in sorghum root and leaf. In this analysis we used the gene expression matrix of the 34K genes annotated in the *S. bicolor* v. 3.1 Btx623 genome for downstream analysis. The gene co-expression networks were calculated based on pairwise gene correlation on standardized log-transformed expression values, the correlation coefficient matrix generated thereafter contains a *P*-value and adjusted *P*-value (p-adj.) generated from multiple comparison using Benjamini–Hochberg procedure. The SimpleTidy GeneCoEx program workflow is based on tidyverse packages and graph theory that allows users to pre-filter the whole genome expression dataset into a subset of high variance genes with significant *F*-values. The F-statistics value for the bait/known genes (genes known for their function in the relevant biological process) were used as a quality control to determine the variance threshold for downstream analysis. In our case, we chose the genes *SbPYE* and *SbBTS* as bait genes as they possess a strong positive correlation ($r = 0.8$) throughout the time-series (Fig. S8). Based on the clear time-series patterns and numbers of DEGs, we focused on the FeLim and ZnEx treatments for co-expression network analysis in roots and leaves. We ran the network analysis in roots separately for the FeLim and ZnEx expression data, and again with the FeLim and ZnEx expression data combined. Simultaneously, the analysis was for leaf data. The correlation coefficient cut-off ($r = 0.5$) was used as criterion for edge selection for the nodes or co-expressed genes in a particular module (Fig. S8). The Leiden algorithm was then used for detection of highly interconnected nodes (genes) in the module. The resolution parameter of the Leiden algorithm was used for module tightness and optimization to reduce the number of loosely interconnected nodes from the modules and defines a

convenient way to slice large co-expression data for a focal biological process. The output of the co-expression networks generated by SimpleTidy GeneCoEx were visualized using Cytoscape (v. 3.10.1).

Enzyme abundance

We used the curation of the enzymatic complexes from the PlantSEED project (Seaver *et al.* 2018), projecting the annotation onto sorghum homologues. We also include in our predictions any in-paralogs within the gene trees that have a pairwise sequence identity greater than that of the homologues. For estimating the enzyme abundance from transcript abundance, we use gene–protein–reaction rules encoded in the metabolic reconstruction. The score assigned to a reaction (R_{exp, i}) is estimated to be the sum of the abundances of its catalysing enzymes, as shown in Equation {res}.

$$R\_\{exp, i\} = \backslash sum\_\{j = 1\}^{\{u\_\{i\}\}} U\_\{exp, j\}$$

Because all subunits are necessary for an enzymatic complex to form and become active, the abundance of an enzyme, U_{exp, j}, is limited by the availability of the least abundant subunit. Therefore, an enzyme abundance is set to the minimum of the abundances of its subunits (Eq. {enz}).

$$U\_\{exp, j\} = Min(S\_\{exp, k\}) \backslash qquad k = 1, \ldots, s\_\{, j\}$$

Lastly, the abundance of each subunit, S_{exp, k}, is the sum of abundances of all paralogs (P_{exp, l}) encoding the subunit, as the expression of any paralog can contribute to the formation of the parent enzyme (Eq. {subunit}).

$$S\_\{exp, k\} = \backslash sum\_\{l = 1\}^{\{p\_\{k\}\}} P\_\{exp, l\}$$

RESULTS AND DISCUSSION

Transport and distribution of metal ions in root and leaf under Fe and Zn stress

Leaf and root phenotype data were collected from hydroponically grown *S. bicolor* BTx623 at several intervals over a 21-day period of Fe or Zn limitation (FeLim or ZnLim, respectively) and Fe or Zn excess (FeEx, ZnEx, respectively) treatments by comparing the ion concentrations (Fe or Zn) in parts per million (ppm) relative to the control plants at each time point that was sampled. For the Fe treatments, FeLim showed some variation in Fe accumulation in the early time points (1D to 4D) in both leaves and roots, but declined relative to controls at the later time points (7D to 21D), as expected under a Fe deficiency response (Fig. 1a, Fig. S1, Table S1). For ion accumulation phenotypes we noted considerable variation among the three replicates (Figs. S1 and S2), which can be the case from ICP-MS data with low replication (Trimmel *et al.* 2023). However, the fold-change estimates confirm expected trends. The FeLim treatment had the strongest visible phenotype at 21 days, with leaves showing obvious signs of chlorosis (Fig. 1b). Spectrophotometer measurements showed a significant reduction in chlorophyll content from 7 to 21 days (Fig. 1c, Table S1), consistent with visible chlorosis. For the FeEx treatment, the accumulation of Fe in roots exhibited a consistent rise throughout the 21-day period, commencing from Day 4 (Fig. 1a, Fig. S1). In contrast, the FeEx treatment resulted in a downward trend in leaves toward the later time points (Fig. 1a, Fig. S1a), and did not result in any chlorosis (Fig. 1c). A similar pattern was observed in rice subjected to excess Fe stress (Aung *et al.* 2018; Aung & Masuda 2020), wherein the plants adopted a defence strategy of retaining Fe in roots which restricts Fe transport to the shoot, and compartmentalization of excess Fe in the basal part of shoots. Following the 21-day period, we measured plant height at the harvest date to determine the effects of the Fe stress on plant growth and found that both FeEx- and FeLim-treated plants were significantly shorter than control plants (Fig. 1d). However, among the two Fe-stress treatments, the FeEx-treated plants were taller than the FeLim plants, indicating that Fe limitation was an overall greater stress to the plants. Our findings are consistent with a previous study in sorghum (Prity *et al.* 2021) showing that Fe concentration in root and shoot significantly declined in plants under Fe limit stress relative to Fe excess.

The Zn stress treatments resulted in more obvious changes in accumulation of Zn in both leaves and roots compared with the Fe treatments, with a clear increase compared to controls across all time points for the ZnEx treatment (Fig. 1e, Fig. S1e–h). The ZnEx treatment showed a steady accumulation in roots throughout the time points, while Zn build up in leaves was maintained at a constant concentration throughout the time series (Fig. S1e). Limiting the supply of excess Zn from the roots to the aerial parts of the plants may decrease the chances of toxicity in the photosynthetic organs. This could be attributed to a defence mechanism to prevent the photosynthesizing tissues from becoming too toxic by retaining excess Zn in the roots. The retention of Zn in roots under Zn excess stress treatment was shown to be a survival strategy in grapevine plants to maintain the homeostatic levels of ions in the photosynthetic tissues (Yang *et al.* 2011). The ZnEx treatments resulted in no visible chlorosis (Fig. 1f) or changes in chlorophyll concentration (Fig. 1g), but it resulted in a significantly reduced plant height compared with control plants (Fig. 1h). For the ZnLim treatment we found a consistent decrease in Zn levels in roots starting from day 1 of treatment and decreases in Zn relative to controls at all time points in leaf and root (Fig. 1e). Under ZnLim treatment, there was a noticeable decrease in Zn accumulation in leaves, particularly after 7 days of treatment. Unlike the FeLim treatment, ZnLim did not result in noticeable chlorosis or decrease in chlorophyll content (Fig. 1f), or significantly shorter plants (Fig. 1h). Similar observations were made by Li *et al.* (2021), wherein a study conducted on *A. catechu* did not find any visible signs of chlorosis in plant seedlings until 80 days post Zn limit treatment.

In the Fe and Zn treatments, we observed other metal ions responding to the treatments, suggesting crosstalk among micronutrient ion transporters. For example, in the FeLim treatment, we found that Zn accumulation was significantly higher than controls at the 4-day and 21-day time points (Fig. S2a), suggesting the co-transport ability of transporter proteins (e.g., *ZIPs*, *IRTs*, *YSL1*, *ZIFLs*) to transport both Fe and Zn ions. Likewise, in the ZnEx treatment, very high levels of Fe were accumulated in leaves at 21-day time point (Fig. S2b) suggesting that transporters translocate both Zn and

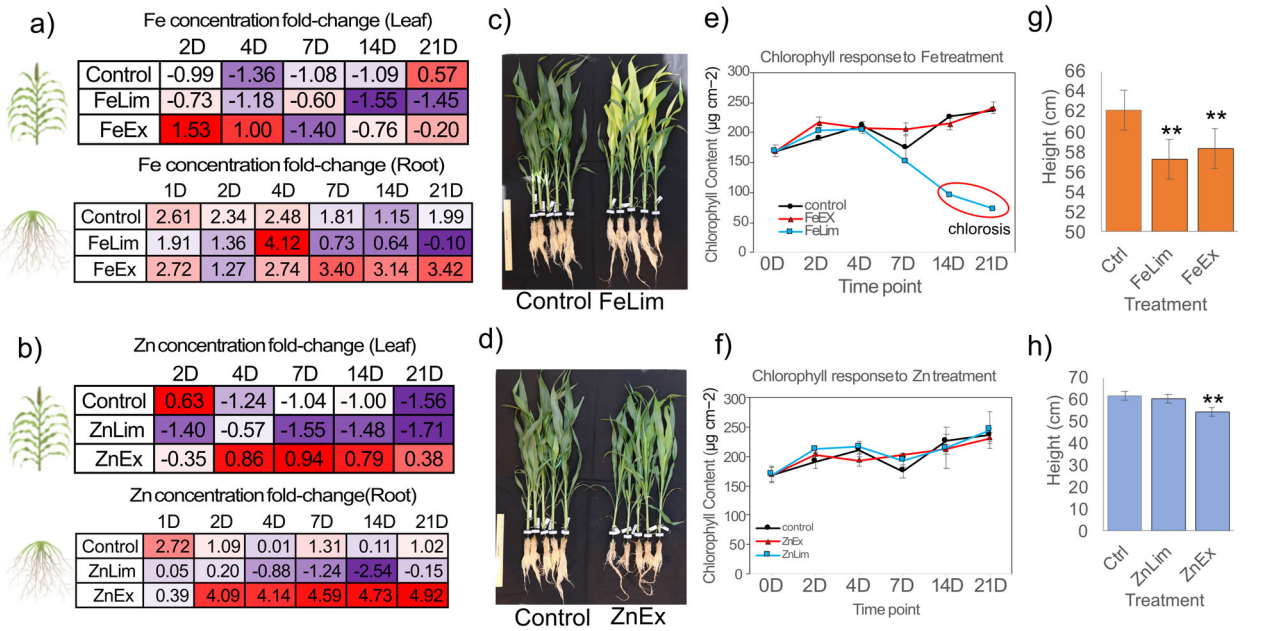

Fig. 1. Heatmaps showing fold-change in Fe concentration compared to control in Fe limiting (FeLim) and Fe excess (FeEx) at each time point in leaf and root tissues (a), and fold-change in Zn concentration compared to control in Zn limiting (ZnLim) and Zn excess (ZnEx) at each time point in leaf and root tissues (b). Numbers in boxes are ratio of treatment over control ppm values. Red indicates an increase in parts per million (ppm) relative to controls, and blue indicates a decrease in ppm relative to control. Sorghum (*S. bicolor cv*. BTx623) harvested after 21 days in FeLim next to plants grown with no treatment (control) (c), and ZnEx compared with control plants (d). Chlorophyll Content Index (CCI) shows changes in chlorophyll over the duration of treatment periods for FeLim, FeEx, control (e) and ZnLim, ZnEx, control (f). Points are mean of 3 biological replicates, error bars are SD of 3 biological replicates at each time point and treatments. Bar graph show plant height for FeLim- and FeEx-treated plants (g) at 21 days and ZnLim and ZnEx at 21 days (h). Bars are means of three biological replicates and error bars are SD of three replicates. Statistical differences in plant height used a two-tail Student *t*-test, significant differences from controls all $P < 0.005$, indicated by asterisks.

Fe under increased Zn availability. Concentrations of micronutrients such as Fe and Zn were also correlated with other micro- and macronutrients under Fe/Zn deficient or excess conditions (Fig. S3b). Based on the ionomic data, visible chlorosis or chlorophyll content, and plant height at harvest date, under the tested conditions, FeLim and ZnEx induced the strongest phenotypic responses to stress. Additionally, these two treatments elicited a response in the other focal ion, such as increased Zn under Fe limitation and increased Fe under the Zn excess treatment, suggesting likely interactions among Fe and Zn gene regulatory processes.

Majority of DEGs were found in Fe limitation and Zn excess treatments

A total of 20,849 genes were found to be differentially expressed (DEGs, defined based on FDR <0.05 and $|\log_2 \text{Fold change}| \geq 1$) when comparing control vs. stress in root and leaf across all time points. When DEGs were further categorized by tissue specificity, we identified 15,255 and 5594 genes that were differentially expressed in leaves and roots, respectively. After further categorizing DEGs based on stress responses in leaves, we found 931 and 9362 DEGs for FeEx and FeLim conditions, respectively, and 4228 and 734 DEGs were found in ZnEx and ZnLim conditions, respectively. This indicated that the FeLim and ZnEx treatments resulted in the majority of DEGs in leaves (Fig. 2a). In roots, we observed 302 and 316 DEGs under FeEx and FeLim treatments, respectively, and 4727 and 249 DEGs under ZnEx and ZnLim treatments, respectively (Fig. 2b). In roots, the majority of DEGs were induced at 2 and 4 days except for ZnEx, where a large number of DEGs were also found at 21 days. Hence, among all the treatments included in the study, only the ZnEx treatment resulted in a substantial number of DEGs in roots. We used RT-qPCR to validate expression of the genes Sobic.009G222200 (*SbOPT3*) and Sobic.001G087700 (*SbBTS*) at all time points, which was shown to be very consistent with RNAseq data (Fig. S4).

Our finding that FeLim and ZnEx treatments induced the strongest transcriptomic response is consistent with the ionomics, chlorophyll content, and plant height measurements, which showed these two treatments resulted in the most obvious changes in phenotypes by the end of the experiment. Moreover, the relatively high number of DEGs in leaves under FeLim suggest it was the most severe stress among all tested treatments, and likely affected photosynthesis and chloroplast function negatively. The temporal expression pattern of the DEGs in leaves showed that most of them were expressed at the later stages (7–21 days) which was consistent with the accumulation pattern of Fe and Zn in leaves. The pattern of DEGs in early and late time points in the leaf tissue is shared by common genes that suggest both immediate and long-term response to stress (Fig. S5). Moreover, in leaves, 1,565 DEGs were shared between FeLim and ZnEx stress (Fig. 2c, Table S2). The DEGs included genes homologous to those known to be involved in photosynthesis (Photosystem b subunits and light

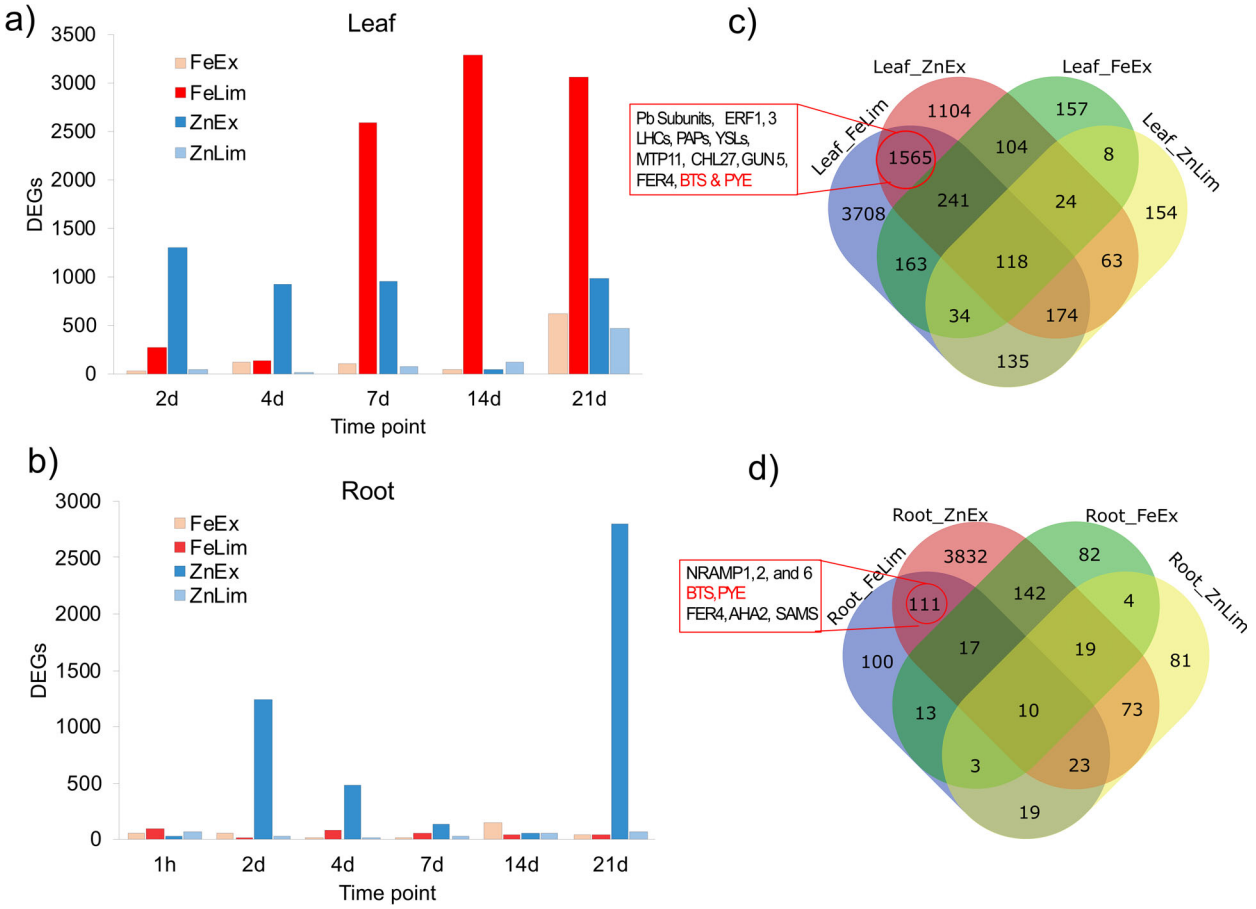

Fig. 2. Number of differentially expressed genes (DEGs) in leaf (a) and root (b) tissues of sorghum, including Fe excess (FeEx), Fe limiting (FeLim), Zn excess (ZnEx) and Zn limiting (ZnLim). y-axes in (a) and (b) are total number of DEGs for each treatment condition, compared with control at each time point. x-axes of (a) and (b) are different time points used for sample collection post-treatment (all time points in days = d, except for root time point: 1 h). Venn diagrams showing number of unique and common DEGs under FeLim, FeEx, ZnLim, and ZnEx treatments in leaf (c) and root (d). DEGs in red box represent common genes between FeLim and ZnEx treatment in leaf (c) correspond to genes involved in chloroplast metabolic process (*SbPS subunit*: Photosystem subunit, *SbLCHs*: Light harvesting complexes, *SbCHL27*, *SbGUN5*: Genome uncoupled 5, *SbPAPs*: 3′-phosphoadenosine-5′-phosphate), metal transporter (*SbYSL*: Yellow stripe-like and *SbMTP11*: *METAL TOLERANCE PROTEIN 11*), transcription factor (*SbPYE*: POPEYE) and E3-ubiquitin ligase (*SbBTS*: *BRUTUS*), and (d) metal ion uptake genes (*SbSAMS*: S-adenosylmethionine synthase, *SbAHA2*: H+-ATPase, *SbNRAMPs*: Natural resistance-associated macrophage protein) in roots and their regulatory genes (*SbBTS* and *SbPYE*).

harvesting complexes, LHCs), chlorophyll biosynthesis (*CHL27* and *GUN5*), retrograde signalling 3′-phosphoadenosine-5′-phosphates (PAPs), along with the known regulators of Fe and Zn homeostasis (*PYE* and *BTS*) (Selote *et al.* 2014; Kroh & Pilon 2020; Akmakjian *et al.* 2021; Sági-Kazár *et al.* 2022). When PAP accumulates due to Fe limitation, it can bind to TFs in the nucleus, initiating upregulation of genes involved in Fe uptake. PAP acts as the primary retrograde signal, accumulating in the chloroplast under Fe stress conditions and then translocating to the nucleus to trigger gene expression changes (Balparda *et al.* 2020).

In roots, there were 111 genes shared between the FeLim and ZnEx treatments, including genes known to be involved in both Strategies I and II (Fig. 2d, Table S3). Among these, the subset of genes included S-adenosylmethionine synthases (*SAMS*), *NICOTIANAMINE SYNTHASE 4* (*NAS4*), Yellow-Stripe-Like proteins (*YSLs*), Zinc-Iron-Regulated-Transporter-Like Proteins (*ZIPs*), and *ZINC-INDUCED FACILITATOR-LIKE 2* (*ZIFL2*) that were previously shown to be involved in the chelation based Strategy II (Kobayashi & Nishizawa 2012). These genes were upregulated at the early time points under both Fe and Zn stress treatments (Figs. 3 and 4a). We also found significant changes in the expression pattern of genes known to be involved in Strategy I, including *Arabidopsis* H^+-ATPases (*AHAs*), Ferric chelate reductases (*FROs*), Natural Resistance-Associated Microphage Proteins (*NRAMPs*), Vacuolar Iron Transporters *VITs*, and Oligopeptide Transporters (*OPTs*) gene families (Kobayashi & Nishizawa 2012; Rai *et al.* 2021; Liang 2022) (Figs. 3 and 4a). The differential expression of the genes for Strategy I were significant only after the plant experienced prolonged exposure to metal stress. The significant changes in the expression pattern of genes as a late response for micronutrient (Fe and Zn) stress suggests the presence of the functional copy of Strategy I genes, and their involvement in combating the stress management in sorghum. A review by Kumar *et al.* (2022) detailed micronutrient uptake and homeostasis in wheat, suggested the transcriptional changes for several of the Strategy I genes under Fe and Zn stress conditions. Similarly, a study by the same group investigating Fe

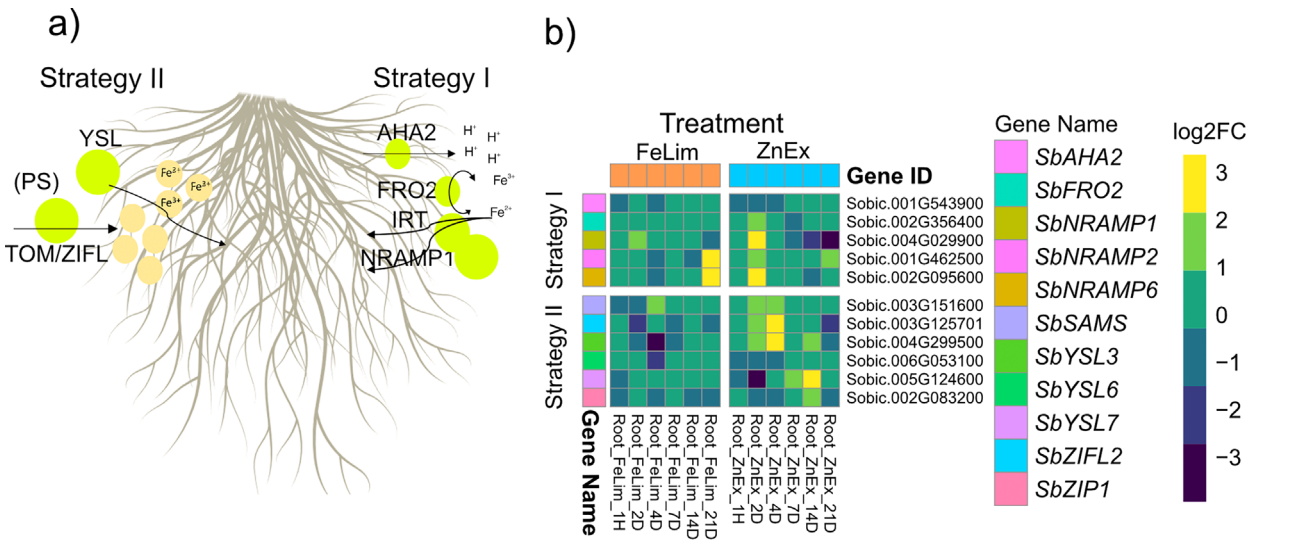

Fig. 3. Illustration of micronutrient (Fe and Zn) uptake by roots, showing genes involved in Strategy I (reduction based) and strategy II (chelation based) (a). The left side of root image depicts Strategy II approach adopted by grasses, where phytosiderophores (PSs) are first released into the rhizosphere by transporters of mugineic acid *TOMs/ZIFLs* followed by uptake of the Fe^{3+} and mugienic acid complex into root by yellow stripe-like transporters (*YSLs*). The right side of root figure depicts the Strategy I found in non-grasses, initiating ion uptake by acidifying the rhizosphere using P-ATPase (*AHA2*) followed by reduction of Fe^{3+} to Fe^{2+} by ferric reductase oxidase (*FRO2*) then its uptake in root by transporters like iron regulated transporter (*IRT*) and/or natural resistant associated macrophage proteins (*NRAMPs*). Upper portion of the heatmap (b) shows expression pattern of Strategy I genes in sorghum root for each time point (1 h, 2 days, 4 days, 7 days, 14 days, 21 days) for FeLim (Fe limiting) and ZnEx (Zn excess) treatments and expression pattern of genes involved in Strategy II are shown in lower heatmap. Gene names are colour coded on y-axis according to gene names listed. Scale bar represents log_2FC gene expression in treated vs. control at each time point, with yellow showing upregulation and dark showing downregulation.

and phosphorus (P) starvation in wheat reported *IRT1* as a key Strategy I gene that supports Fe and P transport and homeostasis in wheat (Kaur *et al.* 2021).

The dual transport of Fe and Zn in sorghum is consistent with previously published studies in *A. thaliana*, where Fe, Zn, Mn, and Cu were simultaneously transported by *IRT1*, *ZIPs*, and *OPTs* (Korshunova *et al.* 1999; Wintz *et al.* 2003; Milner *et al.* 2013), *ZIFLs* in wheat (Sharma *et al.* 2019), and *ZIFLs* and *HMAs* in pearl millet (Goud *et al.*, 2022). In the present study we observed an upregulated expression for *SbZIPs*, *SbVITs*, *SbZIFLs*, *SbOPTs*, *SbYSLs*, and *SbABCGs* transporting Fe and Zn through the common route (Fig. 4a). Similarly, the expression pattern of the transcription factors *SbFIT*, *SbORG2*, *SbPYE*, and *SbBTS* were upregulated in at least for one or two time points after 7 days of FeLim and ZnEx treatment (Figs. 3 and 4b). These results indicated that the DEGs in the leaf and root tissue were consistent with the process of early buildup of Fe stress in roots, initiating transport of ions from roots to shoots. This suggests GRN that underlie transport and compartmentalization due to toxicity in the excess treatments, and photosynthesis impairment in limitation responses (mainly FeLim), which we address using co-expression network analyses later in this manuscript.

We conducted a GO enrichment to further investigate the characteristics of the DEGs for root and leaf tissue from each time point under both Fe and Zn stress treatment. We selected a subset of the complete GO enrichment (Table S4) based on the biological relevance of GO terms to micronutrient stress and grouped them as Fe ion homeostasis-related, ion homeostasis-related, oxidative stress-related, photosynthesis-related, and chloroplast-related (Fig. S6). Enrichment of the Fe-related homeostasis GO terms were shared for the FeEx, FeLim, ZnEx, and ZnLim leaf tissue DEGs at all time points, and for a few time points in the roots (Fig. S6). For the FeEx treatment, the 4-day and 7-day leaf tissue, and 2-day root tissue showed enrichments, and these included shared GO terms in the categories related to Fe ion homeostasis and/or ion homeostasis. The enrichment of the same GO terms at timepoint 2-day in roots followed by 4-day in leaves for FeEx indicated that roots initiated the uptake and transport of ions to leaves in response to stress signals in roots, where leaves promptly responded to maintain ion homeostasis. Consequently, the observed reduction in GO enrichment at later stages in leaf tissue under FeEx stress reflects the plant's ability to restore homeostasis and mitigate the detrimental effects of excess Fe accumulation.

For the FeLim treatment, several GO terms in the chloroplast related category were enriched for the 7-day and 14-day time points in leaves, and FeLim (7-, 14-, 21-day) and ZnEx (2-, 4-day) treatments were enriched for GO terms in the photosynthesis related category for leaf tissues. Moreover, we observed oxidative stress responses in the roots at both early and late time points, attributable to the ZnEx treatment stimulating the production of ROS. Finally, the ZnLim treatment resulted in few GO terms associated with Fe ion homeostasis in leaf tissue and we did not identify any distinct G-terms in the roots under the ZnLim condition. Overall, the GO enrichment provided further confirmation of crosstalk of Fe and Zn metabolic pathways, as suggested by the majority of leaf DEGs induced by the FeLim and ZnEx treatments, as well as shared downstream effects on essential physiological processes, such as photosynthesis and ion homeostasis, as a result of these two treatments.

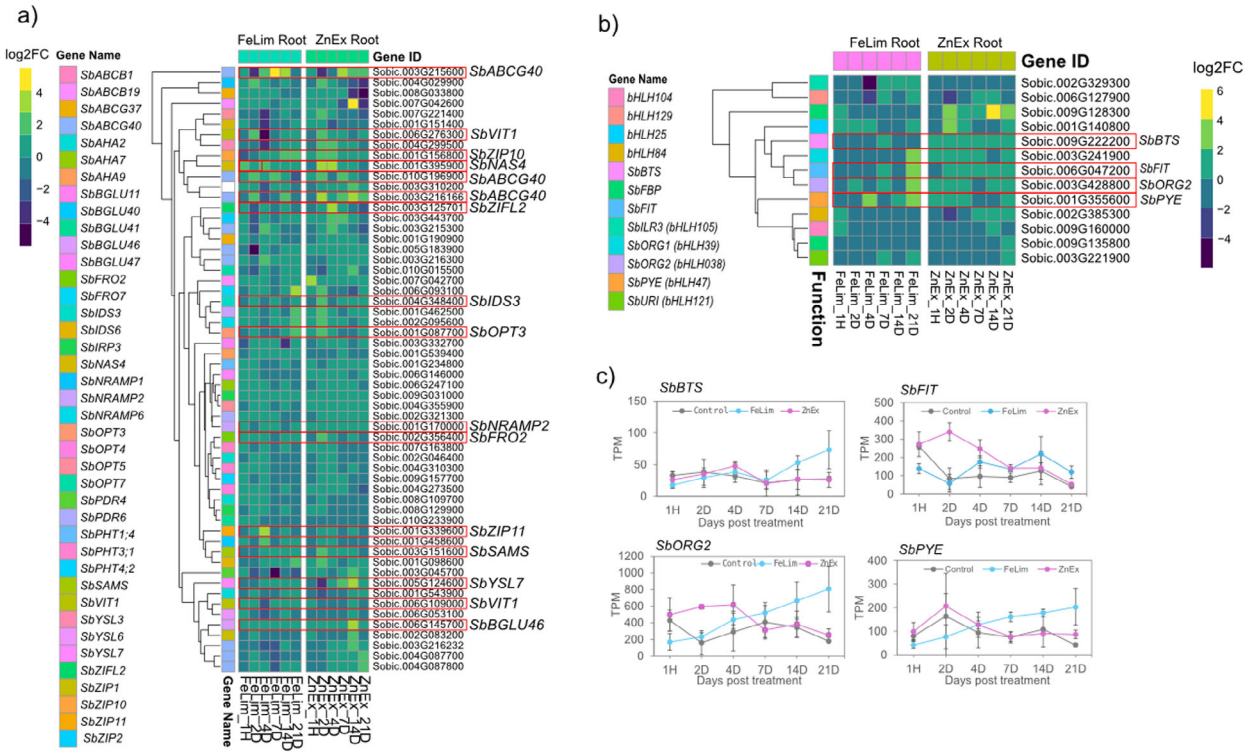

Fig. 4. Heatmap representing DEGs in root under FeLim (Fe limiting) and ZnEx (Zn excess) conditions comprised of (a) transporters and structural genes, and (b) regulatory genes. Columns under each treatment represent time points (1 h, 2 days, 4 days, 7 days, 14 days, 21 days) and treatments (FeLim, ZnEx), the transition in colour change from yellow to dark blue indicates up- and downregulated genes, respectively. Heatmap in left panel (a) shows key genes for Fe and Zn ion homeostasis from both Strategy I and II (*SbAHA2*: P-type ATPase, *SbSAMS*: S-adenosyl methionine synthetase, *SbFRO2*: Ferric oxidase reductase2, and *SbZIP*: Zinc ion permease10 and 11, *SbABCG40*: ATP-binding cassette group40, *SbNRAMP2*: Natural resistance associated macrophage protein2, *SbNAS4*: Nicotinamine synthase4, *SbYSL7*: Yellow stripe like7, *SbZIFL2*: Zinc induced facilitator like2, *SbIDS3*: Iron deficiency3, *SbBGLU46*: Beta-glucosidases46, *SbVIT1*: vacuolar iron transport1, *SbOPT3*: Oligopeptide transporter3). Heatmap in right panel (b) shows key transcription factors (TFs) (*SbPYE*: POPEYE, *SbORG2*: bHLH38, and *SbFIT*: bHLH29) and *SbBTS*: BRUTUS highlighted already known for their role in ion uptake and homeostasis. Genes highlighted by a red box indicate FDR <0.05 in at least 1 time point. Heatmaps were constructed from mean log_2FC expression relative to controls at each time point, yellow to dark blue scale bar represents log_2FC. (c) Line plot showing normalized expression (TPM) profiles of known TFs for their involvement in Fe and Zn uptake and transport.

Differential expression in roots suggests conservation of Fe and Zn stress responses in plants

For many homologues of known Fe and Zn transporters and TFs, we found significant differences in the FeLim and ZnEx gene expression responses relative to control conditions across the entire time series (Fig. S6). Moreover, many of these genes showed upregulation relative to control conditions at each time point, to higher expression levels than the previous time point, particularly under the FeLim condition (e.g., *SbORG2*, *SbPYE*, *SbBTS*, *SbNRAMP1*, *SbNRAMP2*; Fig. 4c, Fig. S7). This suggests strong potential for correlated expression patterns the comprise the co-expression networks. The upregulation of known key ion transporters, such as *SbVIT1*, *SbZIP10*, *SbOPT3*, and *SbNRAMP2*, suggests they are involved in metal ion uptake and are regulated by TFs (*SbFIT*, *SbORG2*, and *SbPYE*). We identified significant expression changes of TFs belonging to the bHLH family, indicating their involvement in regulating the genes (i.e., transporters) for Fe and Zn transport and homeostasis. Among the previously reported bHLH family of TFs involved in metal ion uptake and homeostasis (Zhang *et al.* 2015; Li *et al.* 2019) we observed upregulated expression of *S. bicolor* homologues of bHLH038 (*SbORG2*), bHLH039 (*SbORG1*) (group Ib), bHLH029 (*SbFIT*) (group IIIa), bHLH025 (group IVa), bHLH047 (*SbPYE*) (group IVb) (Fig. 4b,c, Table S5). Apart from the TFs, we also found the continuous upregulation of *BRUTUS* (*BTS*), an E3 ubiquitin ligase that acts as a Fe binding sensor that negatively regulates metal acquisition proteins under metal replete conditions. The role of *BTS* is well characterized as a negative regulator for PYE (bHLH047) proteins. Under Fe deficient conditions BTS (E3 ubiquitin ligase) interacts with *PYE* and initiates its degradation via ubiquitin proteasome pathway in *A. thaliana* (Long *et al.* 2010; Kobayashi *et al.* 2013; Rodríguez-Celma *et al.* 2013; Hindt *et al.* 2017; Stanton *et al.* 2023) and rice (Kobayashi *et al.* 2013; Guo *et al.* 2022; Vélez-Bermúdez & Schmidt 2023). The gene expression profiles of the candidate genes and TFs involved in metal acquisition in roots strongly suggest the conservation of common genetic mechanisms in plants for acquisition of Fe and Zn under deficient or excess conditions.

GRN for Fe and Zn homeostasis in sorghum roots

To understand the relationships between genes and transcription factors involved in metal ion transport, we conducted GRN analysis. Our analysis in the previous DEGs section

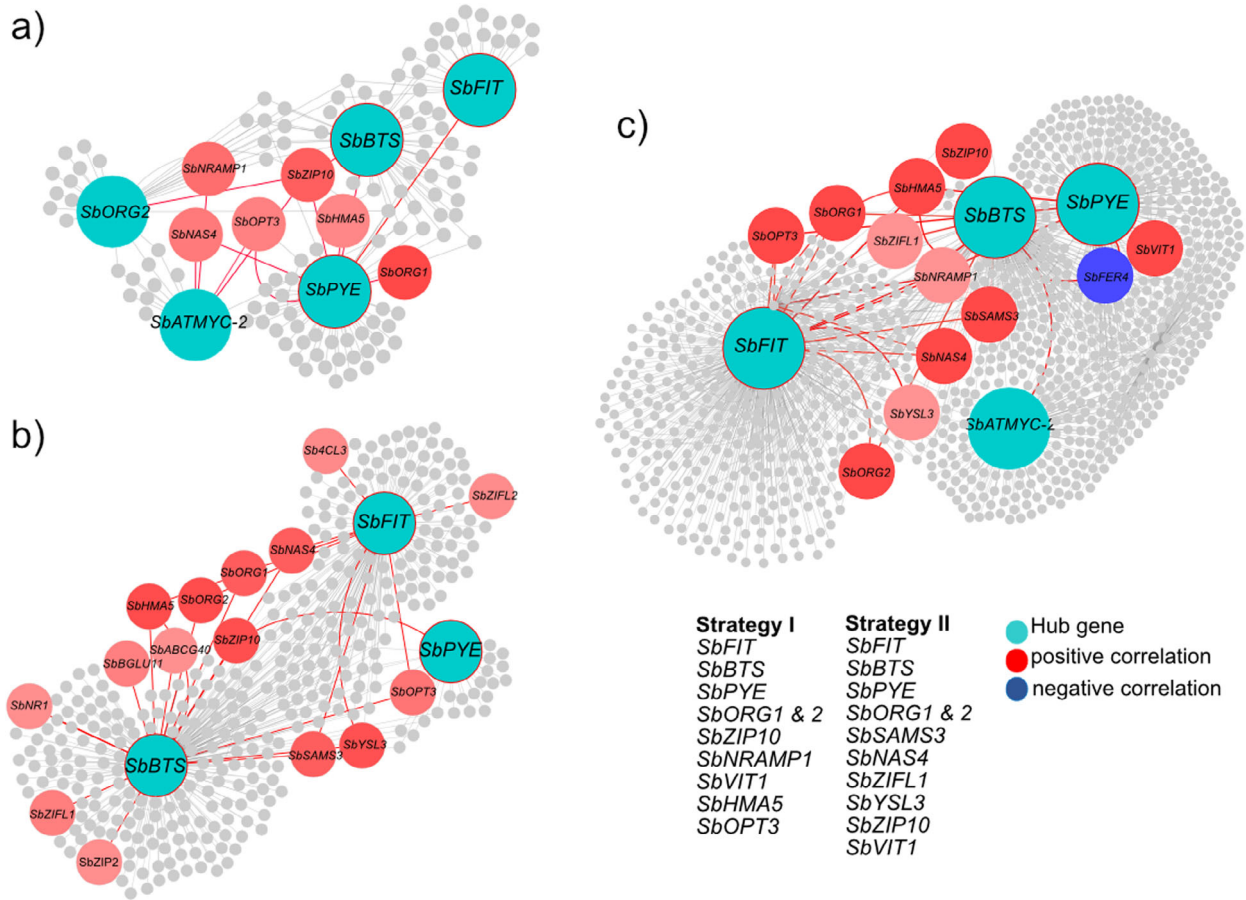

Fig. 5. Gene regulatory network (GRN) analysis of sorghum roots using gene expression from (a) FeLim (b) ZnEx, and (c) combined gene expression from both FeLim and ZnEx treatments. Networks constructed using *SbPYE* and *SbBTS* as bait genes. Solid grey colour circles in each network represent nodes (genes) and large turquoise circles represent hub genes. Nodes labelled with gene names represent genes involved in Fe and Zn homeostasis. Solid red lines were used to highlight connection between bait genes and nodes of interest. Transition in colours of nodes (red is positive and blue is negative) indicate strength of correlations. Correlation coefficient calculated based on mean *z*-score and adjusted *P*-value <0.05.

identified genes that responded to both FeLim and ZnEx, providing support for conservation of Fe and Zn homeostasis genes in plants. This was observed for the genes and transcription factors in both FeLim and ZnEx stress conditions. Therefore, we focused on constructing regulatory networks between the genes that showed a strong connection with their upstream regulatory factors, notably, the upstream regulators *SbPYE* and *SbBTS*. The time-series trend for *SbPYE* and *SbBTS* showed a positive linear correlation ($r = 0.8$; Fig. S7). Our findings are consistent with a previous co-expression network analysis in *A. thaliana* generated using the ATTED II database for Fe stress responses, which showed that *PYE* interacts with *BTS* (Long *et al.* 2010). Considering the expression profiles of *SbPYE* and *SbBTS* in our sorghum datasets and their biological importance in Fe and Zn homeostasis, we used them as bait genes for the co-expression network analysis (Li *et al.* 2023) and their correlations were used to define a cutoff for building GRNs (Fig. S8).

The GRNs showed the interactions between the Fe/Zn upstream regulators *SbPYE* and *SbBTS* and their putative downstream targets involved in Fe and Zn homeostasis (Fig. 5). The GRN analysis using only FeLim gene expression in roots resulted in a total of 19 modules with 3,667 interactions, and ZnEx gene expression in roots resulted in five modules with 3,000 interactions. In both treatment datasets (FeLim only: 19 modules and ZnEx only: 5 modules), *SbPYE* and *SbBTS* were found together in the same modules, suggesting their involvement in regulating both Fe and Zn uptake and transport (Fig. 5a,b, Tables S6 and S7). Visualization of the individual co-expression modules for FeLim and ZnEx treatments showed *SbBTS*, *SbPYE*, and *SbFIT* as common hub genes (Fig. 5a,b). These hub genes showed connections with genes from both Strategy I (*SbORG1*, *SbORG2*, *SbNRAMP1*, *SbHMA5*, *SbABCG40*, *Sb4CL3*) and Strategy II (*SbORG1*, *SbORG2*, *SbSAMS*, *SbNAS4*, *SbZIFL1*, *SbOPT3*, *SbZIP10*, *SbYSL3*) and the correlations were positive. Next, we aimed to identify shared gene interactions by combining the FeLim and ZnEx gene expression data into a single dataset for constructing a GRN. The network analysis showed *SbBTS*, *SbPYE*, *SbFIT*, and *SbMYC-2* as the hub genes interacting with 1,238 nodes (genes), including *SbORG2*, *SbORG1*, *SbSAMS*, *SbNAS4*, *SbZIFL1*, *SbZIP10*, *SbHMA5*, *SbVIT1*, *SbNRAMP1*, *SbYSL3* (Fig. 5c, Table S8). The co-expression network constructed in the present study suggests an overlap between the

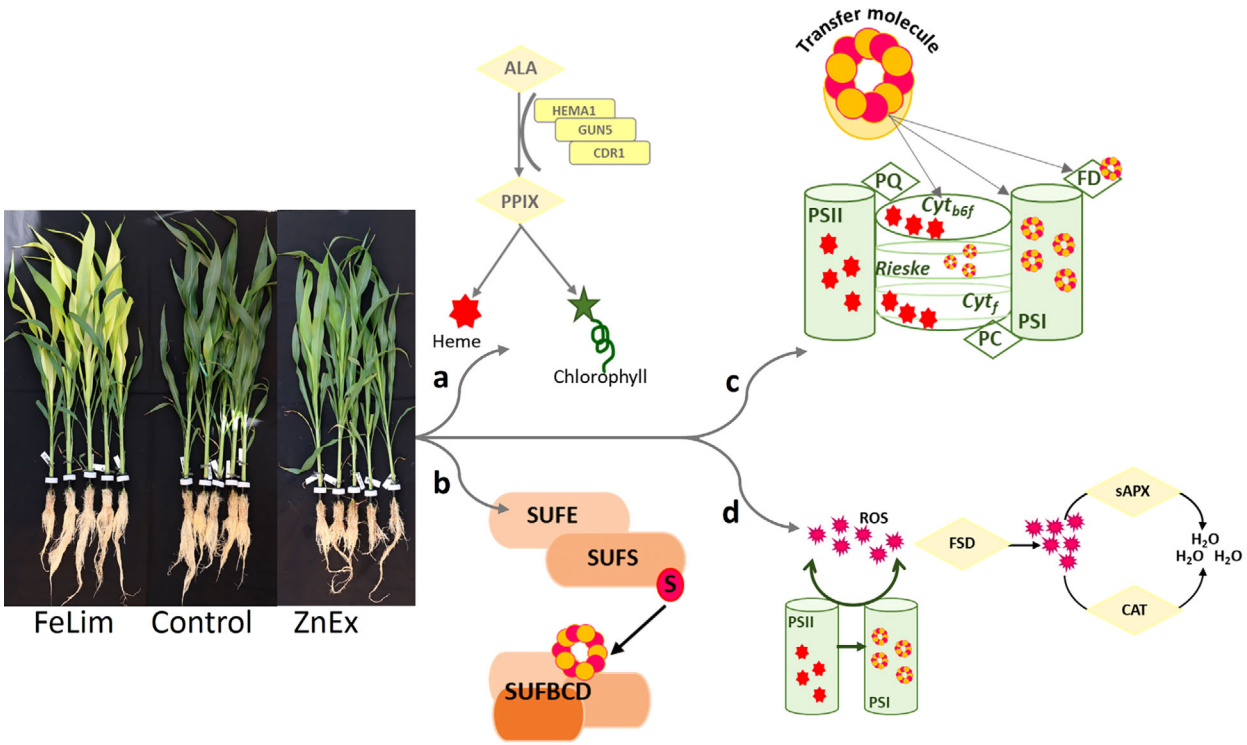

Fig. 6. A schematic representation of leaf metabolic processes affected by FeLim and ZnEx treatment in sorghum leaves, characterized by (a) chlorophyll biosynthesis, (b) Iron sulfur (2Fe-S) cluster assembly, (c) photosynthesis, and (d) reactive oxygen species (ROS) scavenging.

transportation of Fe and Zn using common transporters and TFs, indicating crosstalk.

Regulation of genes in response to Fe and Zn stress in leaf chloroplast

Chloroplasts are a sink for Fe and Zn, and they accumulate most of the available free Fe and Zn ions in leaves. Limited or excess Fe and Zn results in disruption of metabolic processes in chloroplasts, such as chlorophyll biosynthesis, Fe-S cluster assembly, and photosynthesis (Fig. 6). Fe acts a catalyst and is involved in the formation of aminolevulinic acid (ALA), the precursor molecule in chlorophyll biosynthesis and other tetrapyrrole derivatives. Therefore, low availability of Fe in the chloroplast negatively impacts chlorophyll biosynthesis (Fig. 6a). The chloroplasts deprived of Fe-cofactors specifically impair proper functioning of the Fe-S cluster assembly (Fig. 6b). It was found that any defect in plastidial Fe-S assembly resulted in lethal phenotypes in *A. thaliana* (Nakamura *et al.* 2013). Photosynthesis is a multi-component machinery composed of PSI, PSII, Cytb6f, and Rieske proteins involved in photosynthetic electron transport (Fig. 6c), and any alteration in the chlorophyll biosynthesis and Fe-S cluster can lead to disruption of photosynthetic activity (Allen *et al.* 2008). Furthermore, Fe stress in chloroplasts leads to generation of ROS, causing oxidative damage. The ROS generated by impaired photosynthetic activity is neutralized by a ROS scavenging process led by Fe superoxide dismutase (FSD) (Fig. 6d). To understand the physiological consequences of FeLim and ZnEx stress in leaf chloroplasts, we investigated the expression dynamics of the genes involved in the process. In leaves, 9,362 and 4,228 genes were differentially expressed under FeLim and ZnEx treatments, respectively, and most of them were expressed in later stages (7–21 days) post-treatment (Fig. 2a, Table S9).

Chloroplast metabolism appears to be re-modelled in response to Fe and Zn stress in sorghum leaves, as indicated by the downregulation of genes encoding enzymes involved in heme and chlorophyll biosynthesis. The FeLim and ZnEx stress conditions resulted in significant changes in expression in transporter and structural genes involved in chlorophyll biosynthetic processes (Fig. 7a, Fig. S9). *SbHEMA1*, which encodes an enzyme needed for 5-aminolevulinic acid (ALA) synthesis in the tetrapyrrole pathway, was nine-fold down regulated under FeLim and up to three-fold downregulated in ZnEx conditions. In addition, genome uncoupled 5 (*SbGUN5*), a gene known to be involved in chlorophyll production, was also found to be <1.5-fold downregulated (Figs. 6a and 7a). An early response for metal ion stress in *A. thaliana* was also shown by the downregulation of *HEMA1* and *GUN5* involved in chlorophyll biosynthesis (Rodríguez-Celma *et al.* 2013), which supports the pattern observed here.

Our differential expression data suggest that the second major metabolic pathway affected by Fe stress was the chloroplast Fe-S assembly (Fig. 6b). The SUFBCD complex in the assembly comprises multiple SUF-subunits, such as *SUFB*, *SUFC*, *SUFD*, *SUFS*, *SUFE*, and *SUFA* (Xu *et al.* 2005; Liang *et al.* 2014). The *SUFB* subunit of the SUFBCD complex is considered most essential in land plants and was also downregulated at early stages at both transcript and protein levels under Fe stress (Xu *et al.* 2005; Hantzis *et al.* 2018). Following Fe and Zn stress, we identified about two-fold downregulation of the *SbSUFB* subunit. The chloroplast sulfur mobilization protein

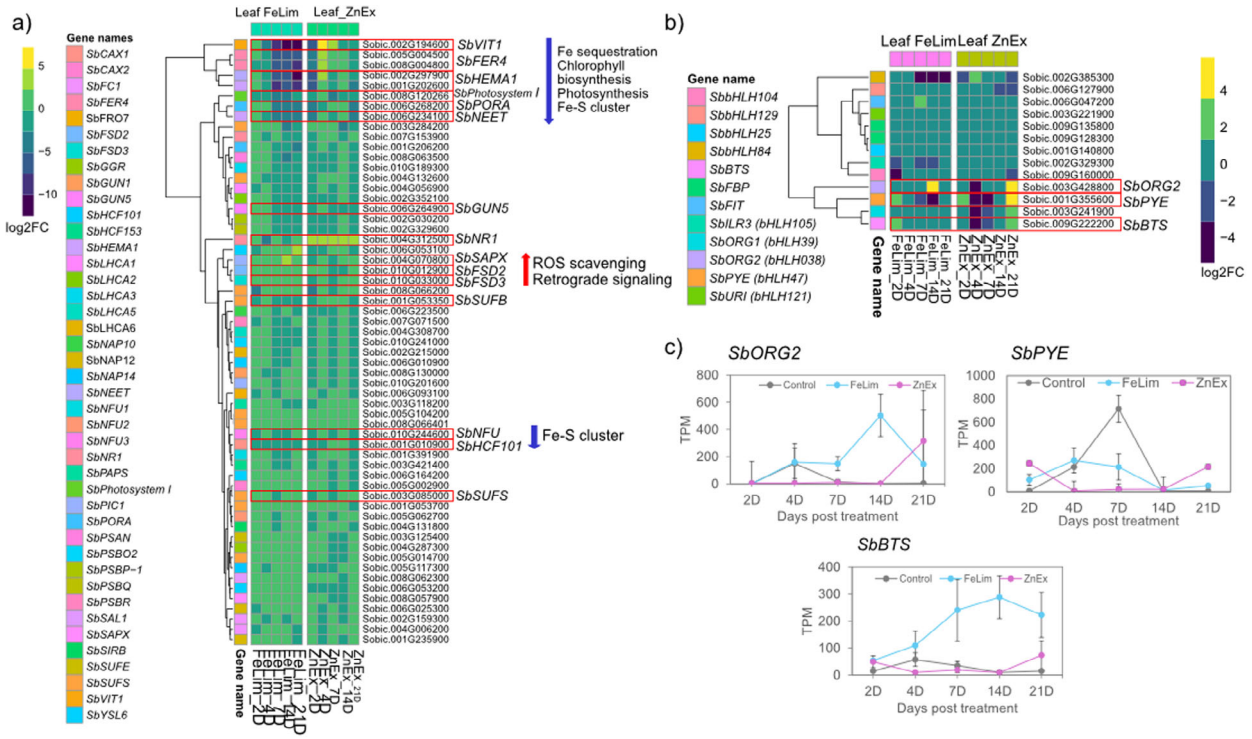

Fig. 7. Heatmap representing DEGs in leaf under FeLim and ZnEx condition for (a) structural genes and (b) regulatory genes. Heatmap in (a) shows cluster of genes involved in leaf metabolic process including ROS scavenging, retrograde signalling, 2Fe-S assembly, chlorophyll biosynthesis and photosynthesis (each component shown in Fig. 6), red and blue upward and downward arrows highlight clusters of up- and downregulated gene expression associated with the process. Heatmap in (b) shows expression of regulatory genes in leaves. Columns under each treatment represent time points and treatment; transition in colour change from yellow to dark blue indicates up- and downregulated genes, respectively. Genes highlighted by a red box indicate FDR <0.05 in at least one time point. Heatmaps constructed using $\log_2$FC expression relative to controls at each time point. (c) Line plot showing normalized expression (TPM) profiles of highlighted regulatory genes in the current study, also reported previously in literature for their involvement in Fe and Zn uptake and transport.

(*SUFS*), also known as N-fixation S-like (*NIFS*) genes, are involved in plastidial assembly of the Fe-S cluster. Silencing of *NIFS* using RNAi was found to be lethal in *A. thaliana*, showing reduced Fe-S cluster formation in plastids (Van Hoewyk *et al.* 2007). In addition to SUF subunits, other components of the Fe-S machinery include N fixation unit (*NFU*) along with high chlorophyll fluorescence 101 (*HCF101*), which are involved in translocation and maturation of SUFs. Both *SbNFU* and *SbHCF101* were significantly downregulated (Fig. 7a), suggesting defective assembly of the Fe-S protein clusters (Figs. 6b and 7a). Finally, *NEET* is the plastidial and mitochondrial localized protein known to be involved in export of Fe-S complex in chloroplasts, and the expression of *SbNEET* showed significant 12-fold (FeLim) and six-fold in ZnEx downregulation (Fig. 7a). The expression of *SbNEET* in leaf tissue was also found to be downregulated in *A. thaliana* grown under Fe-deficient conditions, indicating their coordinating role between chlorophyll biosynthesis and ROS detoxification (Nechushtai *et al.* 2012; Rodríguez-Celma *et al.* 2013).

Photosynthesis is driven by a multi-component complex composed of photosystem II, cytochrome *b6f*, and photosystem I (Fig. 6c). The photosystem II genes are nuclear-encoded and designated as '*PSBs*', along with the light harvesting complex (*LHC*) genes. It is known that the proteins encoded by *PSBs* and *LHCs* function together in binding chlorophyll to thylakoid antenna in order to prepare the PSII reaction center for photosynthesis (Hurt & Hauska 1981; Ben-Shem *et al.* 2003). Related to these processes, we identified a two-fold downregulation at later stages (7–21 days) of the stress response in the genes: *PSBO2*, *PSBP1*, *PSBR* encoding PSII subunits and *LHCs*. The downregulation of these important PSII genes suggests low availability of chlorophyll molecules for binding in the photosystem reaction center. A similar response for *A. thaliana* was observed by Hantzis *et al.* (2018), suggesting a disruption in PSI and PSII along with decreased transcripts and protein abundance for the PS-associated genes under Fe deficiency. Cytochrome *b6f*, which is involved in electron transfer from PSII to PSI was two-fold downregulated under both FeLim and ZnEx stress. Because PSII and cytochrome *b6f* were downregulated and not able to transfer electrons to PSI, we speculate that this disrupts the PSI machinery for energy production, resulting in downregulation of the expression of PSI (*PSAN* and *PSAA*) (six-fold) subunit and *LHCs* (two-fold) genes (Figs. 6c and 7a), consistent with RNAseq patterns of the Fe-deficiency response in *A. thaliana* leaves (Rodríguez-Celma *et al.* 2013).

The disruption in photosynthetic activity and chlorophyll biosynthesis in response to Fe and Zn stress also provides a platform for oxidative damage caused by ROS and the genes involved in ROS scavenging pathways (Fig. 6d). Consistent with ROS damage, iron superoxide dismutase (*SbFSD*) was two-fold upregulated and stromal ascorbate peroxidase (*SbASPx*) was ~1.5-fold upregulated. Catalase (*SbCAT*) 1, the

peroxide metabolizing gene, known to have a lower affinity for hydrogen peroxide (H_2O_2), was downregulated (Fig. 7a). In summary, the downregulation of the genes from the chloroplast metabolic processes that are mainly involved in chlorophyll biosynthesis, photosynthesis, and Fe-S cluster assembly are the likely cause of the chlorotic phenotype. Moreover, the upregulation of genes involved in the ROS scavenging process suggest their role in neutralizing the toxic effects of ROS produced in leaves due to stress.

Metabolic modelling of chlorophyll enzyme complexes

We extended our analysis by examining the DEGs from the leaves in the context of enzyme complexes involved in photosynthesis and chlorophyll biosynthesis. We used the curation of the PlantSEED project (Seaver *et al.* 2018) to identify the subunits involved in the enzyme complexes of these pathways, and we modify our prior approach for estimating the abundance of enzymes from the paralogous transcripts of the subunits (Seaver *et al.* 2014; Methods). We compared enzyme abundances in control condition to the experimental condition for each time point (Fig. S10). For each enzyme, we calculated how distant each pair of data points was from the identity line (where there would be no change between the control vs. treated conditions) and across all comparisons. We found five enzymes involved in chlorophyll biosynthesis in the 85th percentile (Fig. S11). In these enzymes we found three general trends. First, for ZnEx, there did not appear to be any pattern in the abundance of the enzymes. For FeLim, we found that one enzyme, glutamyl-tRNA reductase enzyme, showed the most significant change, downregulated over time. Glutamyl-tRNA reductase is the product of the *HEMA1* gene that is involved in the first rate-limiting step in chlorophyll and heme biosynthesis. In *A. thaliana*, *HEMA1*, *HEMA2*, and *HEMA3* are involved in encoding glutamyl-tRNA reductase; however, only *HEMA1* is expressed in green tissues (Ilag *et al.* 1994; Kumar *et al.* 1996). This enzyme is the first step in the pathway for chlorophyll and heme biosynthesis, and the implication is that it is a key factor in the onset of chlorosis. Finally, for the other four enzymes, we observed upregulation after 14 days. This implies an ineffectual response to the low flux through the chlorophyll biosynthetic pathway, and the fall in chlorophyll content.

Plastidial transcriptional regulation of Fe and Zn homeostasis

The role of bHLH transcriptional regulation in Fe and Zn homeostasis in roots is well documented (16 bHLH TF family members), but few are known to be expressed in shoots (i.e., leaves), with a specific role in Fe and Zn homeostasis (Hao *et al.* 2021). In our study, expression of the bHLH genes *SbILR3* and *SbPYE* showed two- and four-fold downregulation, respectively, in response to Fe deficiency, while no significant expression changes were observed in leaves for Zn excess (Fig. 7b). Both *SbILR3* and *SbPYE* are required to confer photoprotection during Fe deficiency in leaves to avoid phototoxicity leading to severe chlorosis, as shown in *A. thaliana* by Akmakjian *et al.* (2021), where a loss of function of *SbILR3* and *SbPYE* resulted in photosensitivity and compromised photosynthetic efficiency. Both *PYE* and *ILR3* are known to regulate the transcript expression of plastid-localized *FER* and *NEET* and thereby terminate the chain of synthesizing components for photosynthesis machinery (Nechushtai *et al.* 2012; Li *et al.* 2019). However, in sorghum, our data showed transcript turnover for *SbPYE* and *SbILR3* appeared to be regulated by *SbBTS* (~2-fold upregulation) under both FeLim and ZnEx stress (Fig. 7b). In sorghum it appears that plants manage to evade chlorosis because of the continuous accumulation of Fe in leaves at later stages under excess Zn stress (Fig. 1f) due to the crosstalk between Fe and Zn transport.

GRN for Fe and Zn homeostasis in sorghum leaves

Our GRN analysis in leaves showed that *SbBTS* and *SbPYE* were highly correlated and were found in the same module. The GRN using only FeLim conditions identified 16 modules containing 2547 genes. *SbBTS* and *SbPYE* were found to have connecting edges in module 9 with 245 nodes (genes), which also connected the genes (negatively correlated) *SbHEMA1*, *SbPASF*, and *SbPORA*, which are involved in photosynthesis and chlorophyll biosynthesis (Fig. 8a, Table S10). The presence of the above-mentioned genes together in the same module indicates their combined role in essential metabolic processes to regulate photosynthetic function in leaves under Fe stress. For the ZnEx only condition, our co-expression network analysis identified 18 modules containing a total of 3,996 genes. Among the 18 modules identified, *SbBTS* and *SbPYE* were found to co-express in module 13, along with 81 genes. Focusing on the nodes (genes) interacting with *SbBTS* and *SbPYE*, we identified negatively correlated genes involved in Fe-S cluster and Fe sequestration. In contrast, the metal transporter genes *SbNRAMP2*, *SbNRAMP6*, *SbZIP10*, and *SbOPT3* were positively correlated (Fig. 8b, Table S11). The overall negative correlation of *SbPYE* and *SbBTS* with chloroplast genes suggests a physiological response for Fe- and Zn-induced alterations to photosynthetic activity. Furthermore, a positive correlation of *SbPYE* and *SbBTS* with transporters indicates the repair mechanism, where the transporters recruit available ions from the old tissue to young leaves to help control damage.

To gain statistical power and to compare with the FeLim- and ZnEx-only GRNs (Fig. 8a,b), we combined the leaf expression data for FeLim and ZnEx to examine the combined GRN which may provide a more comprehensive network for Fe/Zn stress of chloroplasts and photosynthetic genes. The combined GRN analysis illustrated how Fe and Zn stress together represses the chloroplast machinery. A single module (Module 2) again had *SbPYE* and *SbBTS* as hub genes with 332 nodes, and they were negatively correlated with genes, such as *SbSbCytb6f*, *SbLHCB6*, *SbPSBR*, *SbPSAF* (photosynthesis), *SbCAO*, *SbPORA*, *SbHEMA1* (chlorophyll biosynthesis), *SbFER4*, and 2Fe-S (Fe-S cluster) (Fig. 8c). The genes involved in ROS scavenging (*SbPAP*, *SbCAT*, *SbFSD*) were found to be positively correlated, along with transporters such as *SbNRAMP2*, *SbNRAMP6*, and *SbOPT3* (Fig. 8c, Table S12). The negative correlation of the genes from photosynthesis, chlorophyll biosynthesis, and Fe-S cluster shows the clear connection with the downregulated expression of these genes under limiting and excess stress. Our differential expression and GRN analyses demonstrated that all four aspects illustrated in Fig. 6a–d were affected, which suggests ability to predict disruption of specific photosynthetic processes using time-series gene expression data. Our results are consistent with the

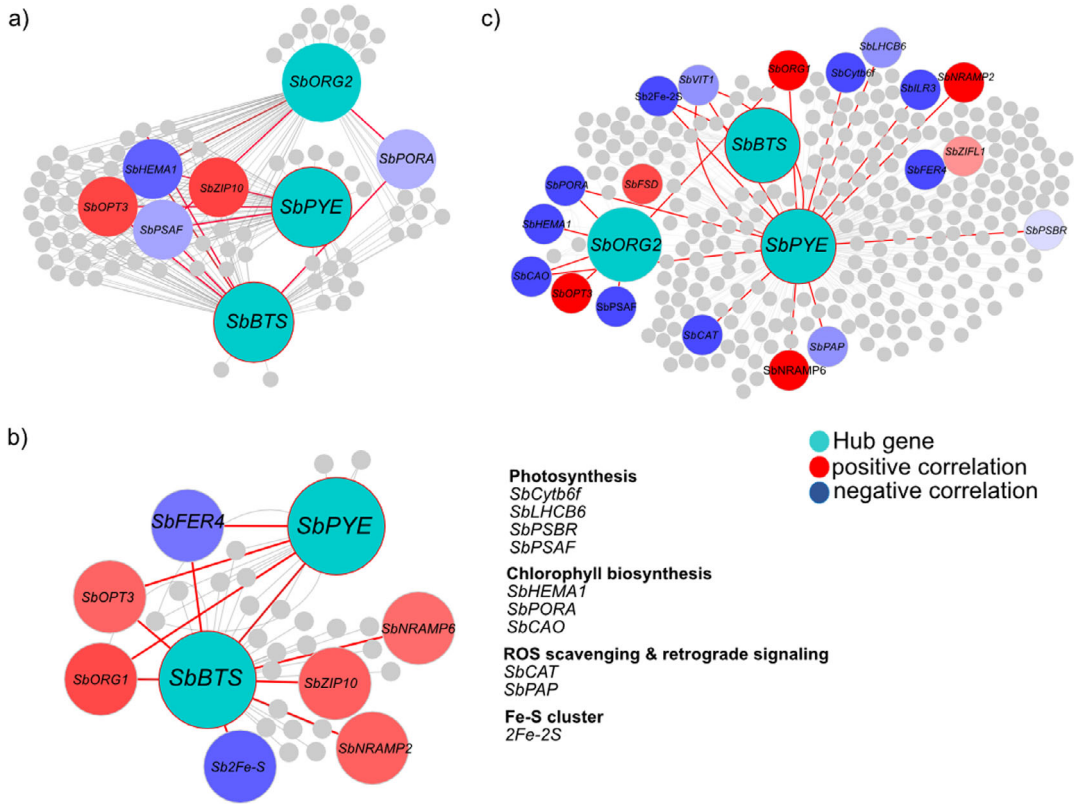

Fig. 8. Gene regulatory network (GRN) analysis of sorghum leaves using gene expression from (a) FeLim (b) ZnEx, and (c) combined gene expression from both FeLim and ZnEx treatments. TNetworks were constructed using *SbPYE* and *SbBTS* as bait genes. Solid grey circles in each network represent nodes (genes) and large turquoise circles represent hub genes. Nodes labelled with gene names represent genes involved in Fe and Zn homeostasis. Solid red lines highlight connection between bait genes and nodes of interest. Transition in colours of nodes (red is positive correlation and blue is negative correlation coefficient) indicate strength of correlations. Correlation coefficients were calculated based on mean *z*-score and adjusted *P*-value <0.05.

previous findings of Burks *et al.* (2022), who used published RNAseq data to construct co-expression networks involved in metabolic processes, such as photosynthesis, fatty acid biosynthesis, plastid organization.

CONCLUSIONS

We observed upregulation of Fe transporters under FeLim conditions resulting in increased uptake and accumulation of Zn and vice-versa, often referred to as cross-talk. In root tissue we found upregulated expression of genes involved in chelator synthesis (*SbSAMS*, *SbNAS4*, and *SbIDS3*) as well as genes involved in intracellular transport of metal chelates including *SbOPT3*, *SbNRAMP2*, *SbABCG37*, and *SbZIP10* which were also upregulated in both root and leaf tissue, suggesting the dual transportation mechanism for Fe and Zn transport in sorghum. The sorghum multi-omic (ionomic and transcriptomic) suggests common routes for Fe and Zn absorption and transportation. In addition to global variation in climate, rainfall, and soil conditions where sorghum grows, intra-seasonal variation is common, particularly in the southern USA, and consists of periods of heavy rainfall during spring seedling growth, followed by drought in mature vegetative and flowering stages of plant growth. We hypothesize that sorghum may use Strategy I mechanism in very wet (flooding) conditions in spring during seedling establishment and utilize Strategy II in hot dry conditions later in the growing season to make Fe bioavailable through a chelation strategy. Future studies are required to test this hypothesis.

The GRN analysis of root responses to FeLim and ZnEx conditions showed that *SbPYE*, *SbBTS* and *SbFIT* were hub genes regardless of separate analyses of the FeLim or ZnEx expression data or when the analysis was done with the combined FeLim and ZnEx expression data. The GRN analysis is supported by what is currently known about regulation of transporters by transcription factors and negative regulators in plant roots, in both non-grass and grass species (Connorton *et al.* 2017; Grillet & Schmidt 2019). Because micronutrient uptake and transport are so fundamental to land plants, it is not surprising to consider the possibility of Fe and Zn GRNs being under strong selective constraints, and highly conserved among non-grasses and grasses. In addition to constraint on belowground processes in plants, we also found *SbPYE* and *SbBTS* were prominent hub genes in the GRN of leaves in sorghum. These were hub genes for regulating genes in (i) chloroplast biosynthesis, (ii) Fe-S cluster assembly, (iii) photosynthesis genes, and (iv) ROS scavenging in the model of chloroplast function (Fig. 6). Because photosynthesis is essential to plant health, growth, and bioproductivity, including plant biomass or grain production, we also expect strong conservation of aboveground processes that affect chloroplast homeostasis among plants.

The sorghum transcriptomics analysis and dataset can serve as a valuable resource for identifying candidate genes for functional genetics studies for trait improvement, such as accumulation of Fe or Zn under deficient or excess conditions, for the bioenergy or sorghum grain agricultural communities. The time-series signal of expression captured in our multi-treatment experiments can be used to generate hypotheses on high impact genes and transcription factors that regulate micronutrient uptake, transport of micronutrients to leaves, crosstalk among essential micronutrients, and how chloroplast metabolic processes can be affected by the expression of these genes. As we have shown, multi-omics datasets can elucidate GRN and metabolic pathways, leading to discoveries on how crops transport important compounds like nutrients and secondary metabolites that enhance quality and resilience. Furthermore, our dataset will lend itself to future studies of comparative GRN analyses across diverse crop species to quantify selective constraints, conservation, and rewiring of micronutrient transport systems. In summary, the integration of multi-omics data is a powerful tool for advancing crop science, improving agricultural practices, and addressing food security challenges.

AUTHOR CONTRIBUTIONS

MX, TP and DW designed the experiment. MX and AB led and conducted the hydroponics experiment, supported by RS, DT, and NG. SK annotated count and normalized read count (TPM) datasets, and conducted ortholog analysis. SK and DW managed raw data submission. AM, TP and NG analyzed phenotype data, and statistical analyses were performed by AM and TP. AM and TP analyzed differential expression data, conducted coexpression analyses, and produced visualizations. RS conducted GO-enrichment. JB analyzed shared differentially expressed genes. MX conducted qPCR validation. SS and SEA conducted enzyme abundance analysis. AM and TP drafted the manuscript, and all authors contributed to final editing and revisions.

ACKNOWLEDGEMENTS

Funding for this project was supported by the U.S. Department of Energy (DOE), Office of Biological and Environmental Research as part of the Quantitative Plant Science Initiative at Brookhaven National Laboratory, USDA-ARS (Project No. 3093-51000-001-000-D). We thank Crysten Blaby for useful comments and suggestions on experimental design, and interpretation of data. We thank Chirag Gupta and Daifeng Wang for early discussions on co-expression network analysis. We thank Charlie Johnson and Marcel Brun at the Texas A&M Genomics and Bioinformatics Service for consultation, sample quality check, sequencing, and initial dataset assembly. We thank Zhanguo Xin and Junping Chen with the USDA Plant Stress and Germplasm Research Development center for useful discussions on data analysis. We thank Michael Clear for bioinformatic analysis and sample quality checks.

DATA AVAILABILITY STATEMENT

The raw sequence data for reads and the processed full normalized expression matrix for each treatment, tissue and time point, with gene annotations and homology to *A. thaliana*, rice, and poplar, is deposited to the National Center for Biotechnology Information (NCBI). The data can be accessible at the BioProject number PRJNA883729 and GSE292584.

SUPPORTING INFORMATION

Additional supporting information may be found online in the Supporting Information section at the end of the article.

Table S1. One-way ANOVA was performed to examine the significant effects of treatments (FeLim, FeEx, ZnLim, and ZnEx) on sorghum root and leaf tissue for accumulation of Fe and Zn ions and leaf chlorophyll content. Below is the output of summary statistics calculated from ANOVA that shows significant effect of treatments at various time points.

Table S2. Functional classification of sorghum DEGs represented in leaves from FeLim and ZnEx stress conditions, representing functional annotation from Arabidopsis ortholog and gene ontology (GO) annotations.

Table S3. Functional classification of sorghum DEGs represented in root from FeLim and ZnEx stress conditions, representing functional annotation from Arabidopsis ortholog and gene ontology (GO) annotations.

Table S4. Gene ontoogy enrichment of DEGs from all treatments in leaves and roots.

Table S5. Table shows the differential expression of genes in sorghum root under FeLim and ZnEx stress. The corresponding annotations for sorghum gene ids were reterived from orthologous search from Arabidopsis using phytozome v3.1.1. The log2FC expression values represents expression for three biological replicates from each time points (1H to 21D) at a threshold of unadjusted *P*-value 0.05 at any time point. The transition in color change from purple to red shows down- and up-regulated genes respectively.

Table S6. Gene regulatory network co-expression summary for sorghum root under FeLim stress condition. The data represented in the table shows the interactions of target (nodes) with source (bait) genes based on pearson's correlation coefficient (Cor (*r*)) calcuated on *z*-scores. The T-statistics was used to calculate *P* value for the correlation coefficient and adjusted *P* value FDR < 0.01 was used to reduce type I error.

Table S7. Gene regulatory network co-expression summary for sorghum root under ZnEx stress condition. The data represented in the table shows the interactions of target (nodes) with source (bait) genes based on pearson's correlation coefficient (Cor (*r*)) calcuated on *z*-scores. The T-statistics was used to calculate *P* value for the correlation coefficient and adjusted *P* value FDR < 0.01 was used to reduce type I error.

Table S8. Gene regulatory network co-expression summary for sorghum root under FeLim and ZnEx stress condition. The data represented in the table shows the interactions of target (nodes) with source (bait) genes based on pearson's correlation coefficient (Cor (*r*)) calcuated on *z*-scores. The T-statistics was used to calculate *P* value for the correlation coefficient and adjusted *P* value FDR < 0.01 was used to reduce type I error.

Table S9. Table shows the differential expression of genes in sorghumleaves under FeLim and ZnEx stress. The corresponding annotations for sorghum gene ids were reterived from orthologous search from Arabidopsis using phytozome v3.1.1. The log2FC expression values represents expression for three biological replicates from each time points (1H to 21D) at a

threshold of unadjusted *P*-value 0.05 at any time point. The transition in color change from purple to red shows down- and up-regulated genes respectively.

Table S10. Gene regulatory network co-expression summary for sorghum leaves under FeLim stress condition. The data represented in the table shows the interactions of target (nodes) with source (bait) genes based on pearson's correlation coefficient (Cor (*r*)) calcuated on *z*-scores. The T-statistics was used to calculate *P* value for the correlation coefficient and adjusted *P* value FDR < 0.01 was used to reduce type I error.

Table S11. Gene regulatory network co-expression summary for sorghum leaves under ZnEx stress condition. The data represented in the table shows the interactions of target (nodes) with source (bait) genes based on pearson's correlation coefficient (Cor (*r*)) calcuated on *z*-scores. The T-statistics was used to calculate *P* value for the correlation coefficient and adjusted *P* value FDR < 0.01 was used to reduce type I error.

Table S12. Gene regulatory network co-expression summary for sorghum leaves under FeLim and ZnEx stress condition. The data represented in the table shows the interactions of target (nodes) with source (bait) genes based on pearson's correlation coefficient (Cor (*r*)) calcuated on *z*-scores. The T-statistics was used to calculate *P* value for the correlation coefficient and adjusted *P* value FDR < 0.01 was used to reduce type I error.

Fig. S1. Concentrations of Fe shown in parts per million (ppm) measured using ICP-MS. Leaf and roots.

Fig. S2. Concentrations of Zn in leaf tissues at each time point following the Fe treatments (a).

Fig. S3. Correlations among micronutrients (Fe, Zn, Mn, Cu, Mo, Na), macronutrients (Ca, K, P, Mg).

Fig. S4. Bar graphs showing real-time quantitative PCR of the *S. bicolor* genes.

Fig. S5. Upset plot illustrating the intersections between the set of DEGs identified in response to Iron.

Fig. S6. Gene ontology (GO) enrichment analysis of DEGs in leaf and root tissues of sorghum.

Fig. S7. Line plot showing the normalized expression (TPM) profiles of candidate genes in root.

Fig. S8. Scatter plots showing standardized *z*-score for BTS (BRUTUS) and PYE (POPEYE) bait genes.

Fig. S9. Histogram showing distributions of Pearson's correlation coefficients (*r*) using leaf FeLim.

Fig. S10. Line plots showing normalized expression (TPM) profiles of candidate genes in leaves. Scale bar to the right of the figure shows distance from diagonal center.

Fig. S11. Change in abundance of enzymes involved in chlorophyll biosynthesis under limited iron.

Fig. S12. List of enzymes involved in chlorophyll biosynthesis that show significant variation.

REFERENCES

Akmakjian G.Z., Riaz N., Guerinot M.L. (2021) Photoprotection during iron deficiency is mediated by the bHLH transcription factors PYE and ILR3. *National Academy of Sciences of the United States of America*, **118**, e2024918118.

Aksoy E. (2024) Barley preferentially activates strategy-II iron uptake mechanism under iron deficiency. *Biotech Studies*, **33**, 23–32.

Allen A.E., LaRoche J., Maheswari U., Lommer M., Schauer N., Lopez P.J., Finazzi G., Fernie A.R., Bowler C. (2008) Whole-cell response of the pennate diatom *Phaeodactylum tricornutum* to iron starvation. *National Academy of Sciences of the United States of America*, **105**, 10438–10443.

Aung M.S., Masuda H. (2020) How does Rice defend against excess iron?: physiological and molecular mechanisms. *Frontiers in Plant Science*, **11**, 1102.

Aung M.S., Masuda H., Kobayashi T., Nishizawa N.K. (2018) Physiological and transcriptomic analysis of responses to different levels of iron excess stress in various rice tissues. *Soil Science and Plant Nutrition*, **64**, 370–385.

Balparda M., Armas A.M., Estavillo G.M., Roschzttardtz H., Pagani M.A., Gomez-Casati D.F. (2020) The PAP/SAL1 retrograde signaling pathway is involved in iron homeostasis. *Plant Molecular Biology*, **102**, 323–337.

Ben-Shem A., Frolow F., Nelson N. (2003) Crystal structure of plant photosystem I. *Nature*, **426**, 630–635.

Burks D.J., Sengupta S., De R., Mittler R., Azad R.K. (2022) The Arabidopsis gene co-expression network. *Plant Direct*, **6**, e396.

Colangelo E.P., Guerinot M.L. (2004) The essential basic helix-loop-helix protein FIT1 is required for the iron deficiency response. *The Plant Cell*, **16**(12), 3400–3412. https://doi.org/10.1105/tpc.104.024315

Connorton J.M., Balk J., Rodríguez-Celma J. (2017) Iron homeostasis in plants – a brief overview. *Metallomics*, **9**, 813–823.

Cooper E.A., Brenton Z.W., Flinn B.S., Jenkins J., Shu S., Flowers D., Luo F., Wang Y., Xia P., Barry K., Daum C., Lipzen A., Yoshinaga Y., Schmutz J., Saski C., Vermerris W., Kresovich S. (2019) A new reference genome for Sorghum bicolor reveals high levels of sequence similarity between sweet and grain genotypes: implications for the genetics of sugar metabolism. *BMC Genomics*, **20**(1), 420. https://doi.org/10.1186/s12864-019-5734-x

Cui Y., Chen C.-L., Cui M., Zhou W.-J., Wu H.-L., Ling H.-Q. (2018) Four IVa bHLH transcription factors are novel interactors of FIT and mediate JA inhibition of iron uptake in Arabidopsis. *Molecular Plant*, **11**(9), 1166–1183. https://doi.org/10.1016/j.molp.2018.06.005

Curie C., Panaviene Z., Loulergue C., Dellaporta S.L., Briat J.-F., Walker E.L. (2001) Maize yellow stripe1 encodes a membrane protein directly involved in Fe(III) uptake. *Nature*, **409**, 346–349.

Eide D., Broderius M., Fett J., Guerinot M.L. (1996) A novel iron-regulated metal transporter from plants identified by functional expression in yeast. *Proceedings of the National Academy of Sciences*, **93**, 5624–5628.

Gaddameedi A., Sheraz S., Kumar A., Li K., Pellny T., Gupta R., Wan Y., Moore K.L., Shewry P.R. (2022) The location of iron and zinc in grain of conventional and biofortified lines of sorghum. *Journal of Cereal Science*, **107**, 103531.

Gao F., Dubos C. (2024) The arabidopsis bHLH transcription factor family. *Trends in Plant Science*, **29**, 668–680.

Goodstein D.M., Shu S., Howson R., Neupane R., Hayes R.D., Fazo J., Mitros T., Dirks W., Hellsten U., Putnam N., Rokhsar D.S. (2012) Phytozome: a comparative platform for green plant genomics. *Nucleic Acids Research*, **40**, D1178–D1186.

Goud C.A., Satturu V., Malipatil R., Viswanath A., Semalaiyappan J., Kudapa H., Rathod S., Rathore A., Govindaraj M., Thirunavukkarasu N. (2022) Identification of iron and zinc responsive genes in pearl millet using genome-wide RNA-sequencing approach. *Frontiers in Nutrition*, **9**, 884381. https://doi.org/10.3389/fnut.2022.884381

Grillet L., Schmidt W. (2019) Iron acquisition strategies in land plants: not so different after all. *New Phytologist*, **224**, 11–18.

Guo M., Ruan W., Zhang Y., Zhang Y., Wang X., Guo Z., Wang L., Zhou T., Paz-Ares J., Yi K. (2022) A reciprocal inhibitory module for pi and iron signaling. *Molecular Plant*, **15**, 138–150.

Hanikenne M., Bouché F. (2023) Iron and zinc homeostasis in plants: a matter of trade-offs. *Journal of Experimental Botany*, **74**, 5426–5430.

Hantzis L.J., Kroh G.E., Jahn C.E., Cantrell M., Peers G., Pilon M., Ravet K. (2018) A program for iron economy during deficiency targets specific Fe proteins. *Plant Physiology*, **176**, 596–610.

Hao Y., Zong X., Ren P., Qian Y., Fu A. (2021) Basic helix-loop-helix (bHLH) transcription factors regulate a wide range of functions in Arabidopsis. *IJMS*, **22**, 7152.

Hindt M.N., Akmakjian G.Z., Pivarski K.L., Punshon T., Baxter I., Salt D.E., Guerinot M.L. (2017) BRUTUS and its paralogs, BTS LIKE1 and BTS LIKE2, encode important negative regulators of the iron deficiency response in Arabidopsis thaliana. *Metallomics*, **9**, 876–890.

Hodnett G.L., Norton S.L., Ohadi S., Bagavathiannan M.V., Rooney W.L. (2020) Wide hybridization and utilization of wild relatives of sorghum. In: Tonapi V.A., Talwar H.S., Are A.K., Bhat B.V., Reddy C.R., Dalton T.J. (Eds), *Sorghum in the 21st century: Food – Fodder – Feed – Fuel for a rapidly changing world*. Springer, Singapore, pp 65–99. http://link.springer.com/10.1007/978-981-15-8249-3_4 [Accessed July 22, 2024]

Hurt E., Hauska G. (1981) A cytochrome f/b6 complex of five polypeptides with Plastoquinol-Plastocyanin-oxidoreductase activity from spinach chloroplasts. *European Journal of Biochemistry*, **117**, 591–599.

Ilag L.L., Kumar A.M., Söll D. (1994) Light regulation of chlorophyll biosynthesis at the level of 5-aminolevulinate formation in Arabidopsis. *The Plant Cell*, **6**, 265–275.

Jacobson L. (1945) Iron in the leaves and chloroplasts of some plants in relation to their chlorophyll content. *Plant Physiology*, **20**(2), 233–245. https://doi.org/10.1104/pp.20.2.233

Kaur G., Shukla V., Meena V., Kumar A., Tyagi D., Singh J., Kandoth P.K., Mantri S., Rouached H., Pandey A.K. (2021) Physiological and molecular responses to combinatorial iron and phosphate deficiencies in hexaploid wheat seedlings. *Genomics*, **113**, 3935–3950.

Khalifa M., Eltahir E.A.B. (2023) Assessment of global sorghum production, tolerance, and climate risk. *Frontiers in Sustainable Food Systems*, **7**, 1184373.

Kim S.A., LaCroix I.S., Gerber S.A., Guerinot M.L. (2019) The iron deficiency response in *Arabidopsis thaliana* requires the phosphorylated transcription factor URI. *Proceedings of the National Academy of Sciences*, **116**, 24933–24942.

Kobayashi T., Nagasaka S., Senoura T., Itai R.N., Nakanishi H., Nishizawa N.K. (2013) Iron-binding haemerythrin RING ubiquitin ligases regulate plant iron responses and accumulation. *Nature Communications*, **4**, 2792.

Kobayashi T., Nishizawa N.K. (2012) Iron uptake, translocation, and regulation in higher plants. *Annual Review of Plant Biology*, **63**, 131–152.

Korshunova Y.O., Eide D., Clark W.G., Guerinot M.L., Pakrasi H.B. (1999) The IRT1 protein from Arabidopsis thaliana is a metal transporter with a broad substrate range. *Plant Molecular Biology*, **40**, 37–44.

Kroh G.E., Pilon M. (2020) Regulation of iron homeostasis and use in chloroplasts. *IJMS*, **21**, 3395.

Kumar A., Kaur G., Singh P., Meena V., Sharma S., Tiwari M., Bauer P., Pandey A.K. (2022) Strategies and bottlenecks in Hexaploid wheat to mobilize soil iron to grains. *Frontiers in Plant Science*, **13**, 863849.

Kumar A.A., Anuradha K., Ramaiah B., Grando S., Frederick H., Rattunde W., Virk P., Pfeiffer W.H. (2015) Recent advances in sorghum biofortification research. In: Janick J. (Ed), *Plant breeding reviews*, Vol. **39**. John Wiley, Hoboken, NJ, 124, pp 89. https://doi.org/10.1002/9781119107743.ch03

Kumar A.M., Csankovszki G., Søll D. (1996) A second and differentially expressed glutamyl-tRNA reductase gene from Arabidopsis thaliana. *Plant Molecular Biology*, **30**, 419–426.

Li C., Deans N.C., Buell C.R. (2023) "Simple tidy GeneCoEx": A gene co-expression analysis workflow powered by tidyverse and graph-based clustering in R. *The Plant Genome*, **16**, e20323.

Li J., Cao X., Jia X., Liu L., Cao H., Qin W., Li M. (2021) Iron deficiency leads to chlorosis through impacting chlorophyll synthesis and nitrogen metabolism in Areca catechu L. *Frontiers in Plant Science*, **12**, 710093.

Li M., Zhang J., Jin H., Feng D., Wang J., Wang H.-B., Liu B. (2019) The iron deficiency response regulators IAA-LEUCINE RESISTANT3 and bHLH104 possess different targets and have distinct effects on photosynthesis in Arabidopsis. *Journal Of Plant Biology*, **62**, 109–119.

Li Y., Zhang Y., Shi D., Liu X., Qin J., Ge Q., Xu L., Pan X., Li W., Zhu Y., Xu J. (2013) Spatial-temporal analysis of zinc homeostasis reveals the response mechanisms to acute zinc deficiency in *Sorghum bicolor*. *New Phytologist*, **200**, 1102–1115. https://doi.org/10.1111/nph.12434

Li X., Zhang H., Ai Q., Liang G., Yu D. (2016) Two bHLH transcription factors, bHLH34 and bHLH104, regulate iron homeostasis in *Arabidopsis thaliana*. *Plant Physiology*, **170**(4), 2478–2493. https://doi.org/10.1104/pp.15.01827

Liang G. (2022) Iron uptake, signaling, and sensing in plants. *Plant Communications*, **3**, 100349.

Liang X., Qin L., Liu P., Wang M., Ye H. (2014) Genes for iron–sulphur cluster assembly are targets of abiotic stress in rice, O ryza sativa. *Plant, Cell & Environment*, **37**, 780–794.

Liang G., Zhang H., Li X., Ai Q., Yu D. (2017) bHLH transcription factor bHLH115 regulates iron homeostasis in *Arabidopsis thaliana*. *Journal of Experimental Botany*, **68**(7), 1743–1755. https://doi.org/10.1093/jxb/erx043

Long T.A., Tsukagoshi H., Busch W., Lahner B., Salt D.E., Benfey P.N. (2010) The bHLH transcription factor POPEYE regulates response to iron deficiency in *Arabidopsis* roots. *The Plant Cell*, **22**, 2219–2236.

López-Millán A.F., Duy D., Philippar K. (2016) Chloroplast iron transport proteins – function and impact on plant physiology. *Frontiers in Plant Science*, **7**, 178. https://doi.org/10.3389/fpls.2016.00178

Mai H.-J., Baby D., Bauer P. (2023) Black sheep, dark horses, and colorful dogs: A review on the current state of the gene ontology with respect to iron homeostasis in Arabidopsis thaliana. *Frontiers in Plant Science*, **14**, 1204723.

Marschner H., Marschner P. (Eds) (2012) *Marschner's mineral nutrition of higher plants*, 3rd edition. Elsevier/Academic Press, Waltham, MA.

Marschner H., Römheld V. (1994) Strategies of plants for acquisition of iron. *Plant and Soil*, **165**, 261–274.

Maurer F., Naranjo Arcos M.A., Bauer P. (2014) Responses of a triple mutant defective in three iron deficiency-induced BASIC HELIX-LOOP-HELIX genes of the subgroup Ib(2) to iron deficiency and salicylic acid. *PLoS One*, **9**(6), e99234. https://doi.org/10.1371/journal.pone.0099234

Milner M.J., Seamon J., Craft E., Kochian L.V. (2013) Transport properties of members of the ZIP family in plants and their role in Zn and Mn homeostasis. *EXBOTJ*, **64**, 369–381.

Mukherjee A., Maheshwari U., Sharma V., Sharma A., Kumar S. (2024) Functional insight into multi-omics-based interventions for climatic resilience in sorghum (Sorghum bicolor): a nutritionally rich cereal crop. *Planta*, **259**, 91.

Mullet J., Morishige D., McCormick R., Truong S., Hilley J., McKinley B., Anderson R., Olson S.N., Rooney W. (2014) Energy sorghum—a genetic model for the design of C4 grass bioenergy crops. *Journal of Experimental Botany*, **65**, 3479–3489.

Nakamura M., Buzas D.M., Kato A., Fujita M., Kurata N., Kinoshita T. (2013) The role of Arabidopsis thaliana NAR1, a cytosolic iron–sulfur cluster assembly component, in gametophytic gene expression and oxidative stress responses in vegetative tissue. *New Phytologist*, **199**, 925–935.

Nechushtai R., Conlan A.R., Harir Y., Song L., Yogev O., Eisenberg-Domovich Y., Livnah O., Michaeli D., Rosen R., Ma V., Luo Y., Zuris J.A., Paddock M.L., Cabantchik Z.I., Jennings P.A., Mittler R. (2012) Characterization of Arabidopsis NEET reveals an ancient role for NEET proteins in iron metabolism. *Plant Cell*, **24**, 2139–2154. https://doi.org/10.1105/tpc.112.097634

Negishi T., Nakanishi H., Yazaki J., Kishimoto N., Fujii F., Shimbo K., Yamamoto K., Sakata K., Sasaki T., Kikuchi S., Mori S., Nishizawa N.K. (2002) cDNA microarray analysis of gene expression during Fe-deficiency stress in barley suggests that polar transport of vesicles is implicated in phytosiderophore secretion in Fe-deficient barley roots. *The Plant Journal*, **30**, 83–94.

Nozoye T., Nagasaka S., Kobayashi T., Takahashi M., Sato Y., Sato Y., Uozumi N., Nakanishi H., Nishizawa N.K. (2011) Phytosiderophore efflux transporters are crucial for iron acquisition in Graminaceous plants. *Journal of Biological Chemistry*, **286**, 5446–5454.

Prity S.A., El-Shehawi A.M., Elseehy M.M., Tahura S., Kabir A.H. (2021) Early-stage iron deficiency alters physiological processes and iron transporter expression, along with photosynthetic and oxidative damage to sorghum. *Saudi Journal of Biological Sciences*, **28**, 4770–4777.

Rai S., Singh P.K., Mankotia S., Swain J., Satbhai S.B. (2021) Iron homeostasis in plants and its crosstalk with copper, zinc, and manganese. *Plant Stress*, **1**, 100008.

Ren G., Yang P., Cui J., Gao Y., Yin C., Bai Y., Zhao D., Chang J. (2022) Multiomics analyses of two sorghum cultivars reveal the molecular mechanism of Salt tolerance. *Frontiers in Plant Science*, **13**, 886805.

Robinson N.J., Procter C.M., Connolly E.L., Guerinot M.L. (1999) A ferric-chelate reductase for iron uptake from soils. *Nature*, **397**, 694–697.

Rodríguez-Celma J., Pan I.C., Li W., Lan P., Buckhout T.J., Schmidt W. (2013) The transcriptional response of Arabidopsis leaves to Fe deficiency. *Frontiers in Plant Science*, **4**, 276.

Sági-Kazár M., Solymosi K., Solti Á. (2022) Iron in leaves: Chemical forms, signalling, and in-cell distribution. *Journal of Experimental Botany*, **73**, 1717–1734. https://doi.org/10.1093/jxb/erac030

Sasaki H., Hirose T., Watanabe Y., Ohsugi R. (1998) Carbonic anhydrase activity and CO_2-transfer resistance in Zn-deficient Rice leaves. *Plant Physiology*, **118**, 929–934.

Seaver S.M.D., Gerdes S., Frelin O., Lerma-Ortiz C., Bradbury L.M.T., Zallot R., Hasnain G., Niehaus T.D., el Yacoubi B., Pasternak S., Olson R., Pusch G., Overbeek R., Stevens R., de Crécy-Lagard V., Ware D., Hanson A.D., Henry C.S. (2014) High-throughput comparison, functional annotation, and metabolic modeling of plant genomes using the PlantSEED resource. *Proceedings of the National Academy of Sciences*, **111**, 9645–9650.

Seaver S.M.D., Lerma-Ortiz C., Conrad N., Mikaili A., Sreedasyam A., Hanson A.D., Henry C.S. (2018) PlantSEED enables automated annotation and reconstruction of plant primary metabolism with improved compartmentalization and comparative consistency. *The Plant Journal*, **95**, 1102–1113.

Selote D., Samira R., Matthiadis A., Gillikin J.W., Long T.A. (2014) Iron-binding E3 ligase mediates iron response in plants by targeting basic helix-loop-helix transcription factors. *Plant Physiology*, **167**, 273–286.

Sharma S., Kaur G., Kumar A., Meena V., Kaur J., Pandey A.K. (2019) Overlapping transcriptional expression response of wheat zinc-induced facilitator-like

transporters emphasize important role during Fe and Zn stress. *BMC Molecular Biology*, **20**, 22.

Spielmann J., Fanara S., Cotelle V., Vert G. (2023) Multilayered regulation of iron homeostasis in Arabidopsis. *Frontiers in Plant Science*, **14**, 1250588.

Stangoulis J.C.R., Knez M. (2022) Biofortification of major crop plants with iron and zinc - achievements and future directions. *Plant and Soil*, **474**, 57–76.

Stanton C., Rodríguez-Celma J., Krämer U., Sanders D., Balk J. (2023) BRUTUS-LIKE (BTSL) E3 ligase-mediated fine-tuning of Fe regulation negatively affects Zn tolerance of Arabidopsis. *Journal of Experimental Botany*, **74**, 5767–5782. https://doi.org/10.1093/jxb/erad243

Suganya A., Saravanan A., Manivannan N. (2020) Role of zinc nutrition for increasing zinc availability, uptake, yield, and quality of maize (*Zea mays* L.) grains: an overview. *Communications in Soil Science and Plant Analysis*, **51**, 2001–2021.

Tabata R., Kamiya T., Imoto S., Tamura H., Ikuta K., Tabata M., Hirayama T., Tsukagoshi H., Tanoi K., Suzuki T., Hachiya T., Sakakibara H. (2022) Systemic regulation of iron acquisition by Arabidopsis in environments with heterogeneous iron distributions. *Plant and Cell Physiology*, **63**, 842–854.

Trimmel S., Meisel T.C., Lancaster S.T., Prohaska T., Irrgeher J. (2023) Determination of 48 elements in 7 plant CRMs by ICP-MS/MS with a focus on technology-critical elements. *Analytical and Bioanalytical Chemistry*, **415**, 1159–1172.

Van Hoewyk D., Abdel-Ghany S.E., Cohu C.M., Herbert S.K., Kugrens P., Pilon M., Pilon-Smits E.A.H. (2007) Chloroplast iron-sulfur cluster protein maturation requires the essential cysteine desulfurase CpNifS. *National Academy of Sciences of the United States of America*, **104**, 5686–5691.

Vélez-Bermúdez I.C., Schmidt W. (2023) Iron sensing in plants. *Frontiers in Plant Science*, **14**, 1145510.

Vert G., Grotz N., Dédaldéchamp F., Gaymard F., Guerinot M.L., Briat J.-F., Curie C. (2002) IRT1, an Arabidopsis transporter essential for iron uptake from the soil and for plant growth. *The Plant Cell*, **14**, 1223–1233.

Vilella A.J., Severin J., Ureta-Vidal A., Heng L., Durbin R., Birney E. (2009) EnsemblCompara GeneTrees: complete, duplication-aware phylogenetic trees in vertebrates. *Genome Research*, **19**, 327–335.

Von Wiren N., Marschner H., Romheld V. (1996) Roots of iron-efficient maize also absorb Phytosiderophore-chelated zinc. *Plant Physiology*, **111**, 1119–1125.

Wairich A., De Oliveira B.H.N., Arend E.B., Duarte G.L., Ponte L.R., Sperotto R.A., Ricachenevsky F.K., Fett J.P. (2019) The combined strategy for iron uptake is not exclusive to domesticated rice (*Oryza sativa*). *Science Reports*, **9**, 16144.

Wang H.-Y., Klatte M., Jakoby M., Bäumlein H., Weisshaar B., Bauer P. (2007) Iron deficiency-mediated stress regulation of four subgroup Ib BHLH genes in *Arabidopsis thaliana*. *Planta*, **226**(4), 897–908. https://doi.org/10.1007/s00425-007-0535-x

Wang N., Cui Y., Liu Y., Fan H., Du J., Huang Z., Yuan Y., Wu H., Ling H.-Q. (2013) Requirement and functional redundancy of Ib subgroup bHLH proteins for iron deficiency responses and uptake in *Arabidopsis thaliana*. *Molecular Plant*, **6**(2), 503–513. https://doi.org/10.1093/mp/sss089

Wintz H., Fox T., Wu Y.-Y., Feng V., Chen W., Chang H.-S., Zhu T., Vulpe C. (2003) Expression profiles of Arabidopsis thaliana in mineral deficiencies reveal novel transporters involved in metal homeostasis. *Journal of Biological Chemistry*, **278**, 47644–47653.

Xu X.M., Adams S., Chua N.-H., Møller S.G. (2005) AtNAP1 represents an atypical SufB protein in Arabidopsis plastids. *Journal of Biological Chemistry*, **280**, 6648–6654.

Yang Y., Sun C., Yao Y., Zhang Y., Achal V. (2011) Growth and physiological responses of grape (Vitis vinifera "Combier") to excess zinc. *Acta Physiologiae Plantarum*, **33**, 1483–1491.

Yuan Y., Wu H., Wang N., Li J., Zhao W., Du J., Wang D., Ling H.-Q. (2008) FIT interacts with AtbHLH38 and AtbHLH39 in regulating iron uptake gene expression for iron homeostasis in Arabidopsis. *Cell Research*, **18**(3), 385–397. https://doi.org/10.1038/cr.2008.26

Zhang J., Liu B., Li M., Feng D., Jin H., Wang P., Liu J., Xiong F., Wang J., Wang H.B. (2015) The bHLH transcription factor bHLH104 interacts with IAA-LEUCINE RESISTANT3 and modulates iron homeostasis in Arabidopsis. *Plant Cell*, **27**, 787–805.

Zhong S., Li X., Li F., Liu T., Pan D., Liu Y., Liu C., Chen G., Gao R. (2022) Source and strategy of iron uptake by Rice grown in flooded and drained soils: insights from Fe isotope fractionation and gene expression. *Journal of Agricultural and Food Chemistry*, **70**, 2564–2573.